Opto-Electronic Advances

Review

2021, Vol. 4, No. 7

DOI: 10.29026/oea.2021.200079

Laser scribed graphene for supercapacitors

Zhengfen Wan, Xi Chen and Min Gu*

Supercapacitors, with the merits of both capacitors for safe and fast charge and batteries for high energy storage have drawn tremendous attention. Recently, laser scribed graphene has been increasingly studied for supercapacitor applications due to its unique properties, such as flexible fabrication, large surface area and high electrical conductivity. With the laser direct writing process, graphene can be directly fabricated and patterned as the supercapacitor electrodes. In this review, facile laser direct writing methods for graphene were firstly summarized. Various precursors, mainly graphene oxide and polyimide were employed for laser scribed graphene and the modifications of graphene properties were also discussed. This laser scribed graphene was applied for electrochemical double-layer capacitors, pseudo-capacitors and hybrid supercapacitors. Diverse strategies including doping, composite materials and pattern design were utilized to enhance the electrochemical performances of supercapacitors. Featured supercapacitors with excellent flexible, ultrafine-structured and integrated functions were also reviewed.

Keywords: Laser; graphene; laser scribed graphene; supercapacitor

Wan ZF, Chen X, Gu M. Laser scribed graphene for supercapacitors. *Opto-Electron Adv* **4**, 200079 (2021).

Introduction

Supercapacitors, also called electrochemical capacitors or ultracapacitors, have been intensively studied over the past few years to meet the rapidly growing demand for highly efficient energy storage devices[1–3]. Owing to their unique advantages including high power density (10 kW/kg), short charge/discharge duration (in seconds), and long cycle life (over 1 million cycles), supercapacitors were considered to be promising candidates in the applications of consumer electronics, hybrid electric vehicles and industrial power management[4,5]. Supercapacitors with high energy and power densities, small sizes, light weights and mechanical flexibility properties have been highly demanded[6–8].

Graphene, a flat monolayer of carbon atoms tightly packed into a two-dimensional (2D) honeycomb lattice, has become a hot research topic since its discovery[9,10]. It shows great potential for supercapacitor applications due to its exceptional high theoretical surface area (2630 $m^2 \cdot g^{-1}$) and electrical conductivity[11]. Many approaches such as mechanical exfoliation[12], chemical vapor deposition (CVD)[13] and the reduction of graphene oxide[14,15] have been developed to produce graphene materials. Recently, a laser direct writing method for graphene has drawn tremendous attention, because of its unique advantages including selective and localized reduction, flexible patterning and no requirement for additional chemicals[16,17]. Based on the laser scribed graphene (LSG), various applications have been demonstrated, including hologram[18], energy storage[19–21], strain sensor[22,23], biosensor[24,25] and antennas[26]. Unlike conventional microfabrication methods such as lithography, this laser technique does not require the utilization of masks, expensive materials, post-processing and cleanroom operations[27–31]. The LSG can be directly prepared by laser irradiation and simultaneously patterned for the elec-

Centre for Artificial-Intelligence Nanophotonics, School of Optical-Electrical and Computer Engineering, University of Shanghai for Science and Technology, Yangpu, Shanghai 200093, China.

*Correspondence: M Gu, E-mail: gumin@usst.edu.cn

Received: 17 November 2020; Accepted: 19 February 2021; Published: 20 July 2021

trodes of supercapacitors. This facile and cost-effective method of graphene fabrication has demonstrated great potential for commercial supercapacitor applications.

In this review, the recent developments of the LSG supercapacitors were summarized. Firstly, we concluded the fabrication and modification of LSG. Particular attention is paid to the application of electrochemical double-layer capacitors (EDLCs), pseudo-capacitors and hybrid supercapacitors, and the diverse strategies to achieve high-performance, flexible, ultrafine-structured and integrated supercapacitors. Current challenges and future advancements of LSG based supercapacitors were also discussed.

Different precursors-graphene oxide, commercial polyimides and other carbon resources were employed for laser scribed graphene production in the literature. The resulting graphene materials are referred differently in scientific reports as laser reduced graphene oxide[32], laser-induced graphene[33], laser-scribed graphene[34], or laser carbonized nanomaterials[35]. The term 'laser scribed graphene (LSG)' is adopted throughout this paper.

Laser scribed graphene

Preparation of laser scribed graphene

Graphene oxide

Graphene oxide (GO), which has the skeleton of graphene decorated with oxygen components, is considered as an important precursor of LSG[15]. It can be produced in large scale by cost-effective chemical methods, forming stable aqueous colloids that are favored by industrial processes[38]. GO films were prepared by spin-coating, drop-casting, blade, or freezing-drying method. Graphene devices on diverse substrates, including leaf, lens, fabrics etc. can be fabricated by laser technology[39]. Xiao et al., fabricated LSG microcircuits with the line widths of 500 nm by the laser irradiation on GO films[32]. Figure 1(a-c) shows the fabrication of GO films and the LSG microstructures, and the scanning electron microscopy (SEM) images of the microcircuits. After the laser writing, the thicknesses of film decrease and the color of film turns to black. An obvious removal of oxygen components can be observed as indicated in AFM and XPS results in Figure 1(d-f). The mechanism of laser reduction of GO was strongly related to the photochemical and photothermal effect of laser[15]. The threshold of GO photoreduction was 3.2 eV (390 nm)[40]. For the laser with wavelength < 390 nm, the photochemical effect of laser can trigger the C–O bonding weakening and the oxygen removal. Meanwhile, it was reported that the exothermic reduction of GO occurs at a temperature between 200-230 °C[41]. The high temperature induced by laser could easily break the C–O and C=O bonds, leading to the reduction of GO. In this laser reduction process, two subprocesses, namely the direct conversion from sp^3 carbon to sp^2 carbon and removal of oxygen functional groups can occur, resulting in the reduced graphene oxide (rGO)[42]. The ultrafast thermal transferred process triggered by the laser spot can also induce the simultaneous exfoliation and reduction of GO, and thereby enhance its specific surface area[43]. Beside GO film, GO in solution, GO fiber and GO aerogel can also be reduced to rGO with laser treatment. Figure 1(g) shows the dramatic color change of the GO solution with ammonia before and after the pulsed laser irradiation[36]. Upon pulsed laser irradiation, the yellow-brown color instantaneously turned black, indicating the effective reduction of GO in solution. GO fiber were also region-specifically reduced by laser irradiation to fabricate a flexible fiber supercapacitor with reduced GO layers as electrodes and GO as the separator[44]. Figure 1(h) shows that a precursor of GO aerogel, after being exposed to a laser spot, was reduced in only tens of milliseconds and converted to graphene bulks[37]. In another report, the self-assembled GO liquid crystals on the surface of GO solutions can also be reduced by laser[45]. Ibrahim et al. introduced the production of reduced GO gels by focusing a femtosecond laser on air/GO solution interfaces[46].

Polymer and biomass

In 2014, Tour's group reported the fabrication of porous LSG films from commercial polymer films using a CO_2 laser[47]. The polyimide (PI) and ployetherimide out of 15 different polymers were successfully converted to LSG under laser irradiation. The LSG with excellent electrical conductivity (5 –25 $S{\cdot}cm^{-1}$) can be readily patterned to interdigitated electrodes for in-plane supercapacitors with specific capacitances of < 44 $mF{\cdot}cm^{-2}$ and power densities of ~9 $mW{\cdot}cm^{-2}$. Figure 2(a-c) shows the laser pattern on PI and the SEM images of LSG, exhibiting high surface area (~340 $m^2{\cdot}g^{-1}$) with pore sizes < 9 nm. The Raman spectrum of LSG (Figure 2d) demonstrates a 2D Raman band (centered at 2 700 cm^{-1}), typically found in that of 2D graphite. The XRD pattern of LSG (Figure

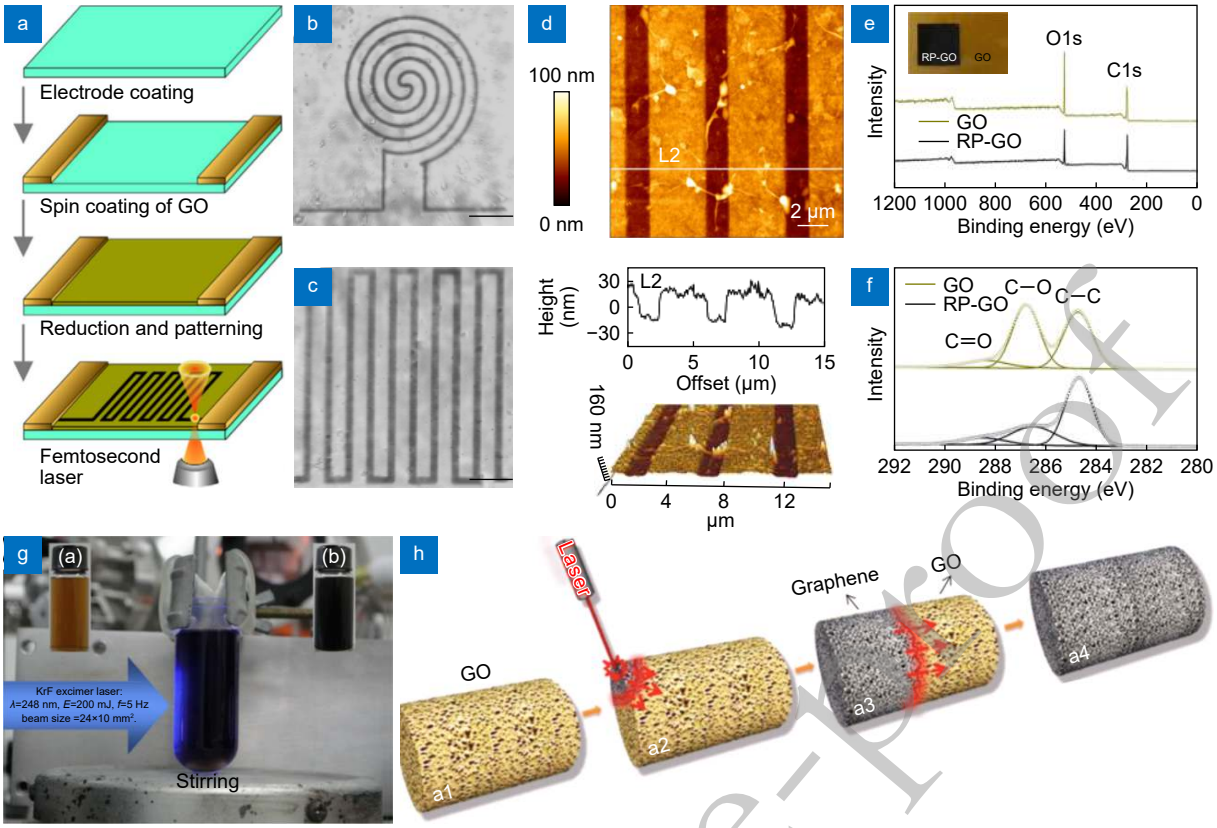

Fig. 1 | Illustration of various GO precursors reduced by laser scrbing. (**a**) The preparative procedure of LSG microcircuit on GO film. (**b-c**) Optical microscopy images of laser patterned microcircuit; Scale bars, 10 μm. (**d**) atomic force microscope (AFM) image of LSG microcircuit on GO film, the height profile along the white line (L2), and its 3D image; (**e**) Survey X-ray photoelectron spectra of GO and LSG, inset is a photograph of a LSG square on a GO film; (**f**) C1s x-ray photoelectron spectroscopy (XPS) spectra of GO and LSG.[32] (**g**) The experimental setup of pulsed laser reduction system. The inset is optical images of GO solution (15 mL 0,1 mg/mL) before (left) and after (right) pulsed laser irradiation.[36] (**h**) Schematic illustration of the GO aerogel treated by laser for the preparation of graphene bulks.[37]

2e) exhibits an intense peak centered at 2θ=25.9°, indicating the high degree of graphitization. This LSG formation is attributed to the extremely high localized temperature (>2500 °C) triggered by the CO_2 laser beam, which can break C–O, C=O and C–N bonds and rearrange the aromatic compounds to graphene structures. In a similar process, Zhang et al., converted phenolic resin into LSG with 3D porous structures, a low resistance (~44 $Ω·sq^{-1}$) and a good mechanical property in large scale by a laser scribing[50]. The polybenzoxazine resin poly (Phddm) with good flexibility, high thermal stability and superior chemical resistance was also employed for the fabrication of LSG by straightforward CO_2 lasing[51]. The graphitization of sulfonated poly(ether ether ketone) (SPEEK) film was obtained for an all-SPEEK flexible supercapacitor using a pulsed CO_2 laser[52]. The resulting LSG can act as the binder-free electrode. The current collector and the SPEEK is employed as both separator and polymeric electrolyte. With laser treatment, natural precursors such as wood[48], cloth, paper, potato skins, coconut shells, cork[49] and lignin[53], which are inexpensive, abundant, and biodegradable, can also be transformed into graphene, as shown in Figure 2(f-j). Kaner et al. converted carbon nanodots (CNDs) into high-surface-area 3D graphene networks with excellent electrochemical properties by an irradiation with an infrared laser[54]. The fabricated 3D LSG electrodes show high specific volumetric capacitance of 27.5 $mF·cm^{-3}$ and extremely fast charging rates with a relaxation time of 3.44 ms.

Modification of laser scribed graphene

The chemical component, structure and morphology of LSG is strongly affected by the laser scribing process and can be modified by adjusting the laser parameters, laser process, laser system, precursors and environment. Laser systems with varied wavelengths, including CO_2 laser (10.6 μm)[35], near-infrared (NIR) laser (1064 nm)[55], 780 nm femtosecond (fs) laser[42] and 405 nm semiconductor laser[56] were reported to fabricate LSG. The laser reduction process is attributed to the photochemical ef-

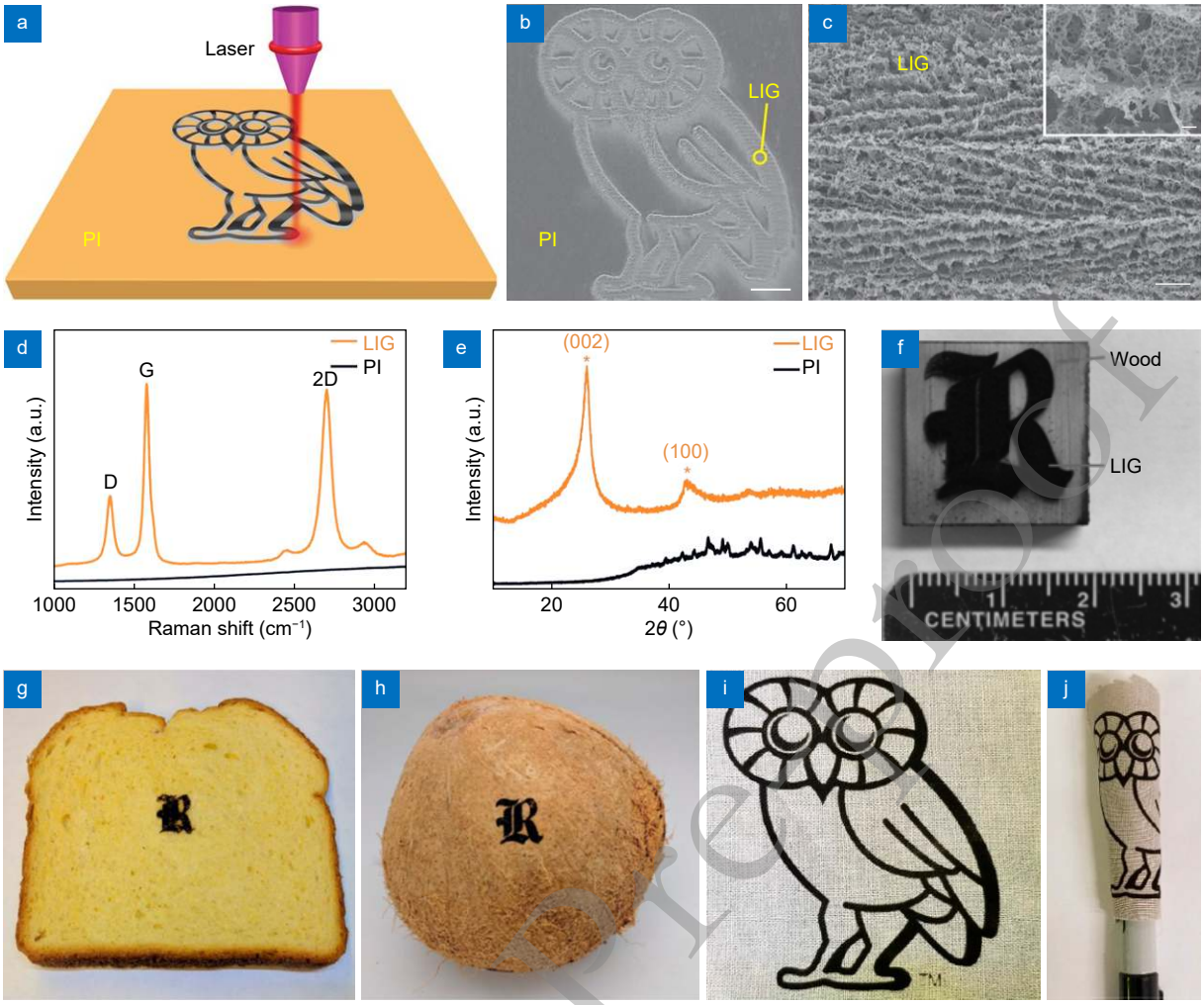

Fig. 2 | (**a**) Schematic illustration of laser patterning on polyimide (PI). (b-c) SEM image of LSG on the PI substrate (**b**) with scale bar 1 mm and its enlarged SEM image with scale bar 10 μm (**c**). Inset is the corresponding SEM image with higher magnification, scale bar 1 μm. (**d-e**) Raman spectrum (d) and X-ray diffraction (XRD) (e) of a LSG and the PI film[47]. (**f**) A photo of LSG on pine wood[48]. (**g**) The letter "R" in LSG induced from bread. (**h**) Picture of LSG patterned into an "R" on a coconut (2 cm tall). (**i-j**) LSG on cloth in the shape of an owl (60 mm in height) (i) and the wrapped cloth (j)[49].

fect and photothermal effect induced by laser[15]. The surface modification of LSG, including modulating the surface morphologies, carbonization and wettability was demonstrated by adjusting laser powers, scanning speeds and pulse repetition frequencies[35,57,58]. Different morphologies, namely "sheet", "needle" and "porous", can be achieved with the optimized laser-writing recipes[59]. With repeated laser irradiations, the structure of PI-derived LSG can be transformed from its original macroporous foam to an intermediate concave corrugated tile structure, and finally a carbon nanotube structure[60]. Instead of a focused round beam, a wide line beam was employed to transform GO into LSG, improving the efficiency of large area laser reduction[61]. The resulting LSG electrode exhibits a high specific capacitance (~130 $F \cdot g^{-1}$) at a current density of 1 $A \cdot g^{-1}$. Sun et al., reported a hierarchical-structuring and synchronous GO photoreduction using a nanosecond laser holography technology[62]. The laser beam was split into two with an equal intensity, and then interfered on the surface of a GO film. The periodic light field patterns generated by the interfered laser beams resulted in the periodic micro-nano structures of LSG. It was found that the laser reduction of PI resulted in self-nitrogen-doped porous LSG (sourcing from the N element of PI precursor), improving its conductivity and electrochemical performance[24]. Guan et al., fabricated the porous LSG without agglomeration by a laser treatment on GO sheets in liquid nitrogen[63]. Due to cryotemperature development and depressed thermal expansion, the frozen LSG exhibits crack-free porous morphologies and shows a decrease of sheet resistance by a factor of 10^4 to 10^5. By controlling the laser reduction atmosphere

(O_2, air, Ar, H_2, and SF_6), the water contact angle of LSG was modulated from 0° (O_2 or air) to >150° (Ar or H_2) or >160° (SF_6)[64].

Laser scribed graphene based supercapacitor

Based on the different energy storage mechanisms, supercapacitors (SCs) can be divided into two types: electrochemical double-layer capacitors (EDLCs) and pseudo-capacitors[65]. EDLCs, which are non-Faradaic capacitors, store energy by building up charges in the layers of the electrical double-layer formed at the interface of electrode/electrolyte[66]. Owing to the fast physical charging and discharging process, EDLCs show great advantages of short charging time, high power densities and long lifespans. However, the capacitance of EDLCs is relatively low due to the limited effective surfaces of electrodes. In this way, LSG electrodes with excellent conductivities and high surface areas are very promising to improve the energy density of EDLCs. Different from EDLCs, the capacitance of pseudo-capacitors is acquired from the storage of charge in the bulk of a redox material following a redox reaction[65]. This fast redox reaction acts like capacitance (hence the name pseudo-capacit-

Table 1 | The performances of laser scribed graphene based supercapacitors

Laser	Precusor	Substrate	Structure	Electrolyte	Supercapacitor performance					Refer.
					Voltage (V)	C_A (mF·cm^{-2})	C_V (F·cm^{-3})	E_V (mWh·cm^{-3})	P_V (W·cm^{-3})	
LightScribe DVD optical drive	GO film	PET	Sandwich	PVA/H_3PO_4	1	N/A	0.4	0.04	1	68
				$TEABF_4$	3	4.82	N/A	0.4	10	
				BMIM-BF_4	4	5.02	N/A	0.8	10	
LightScribe DVD optical drive	GO film	PET	In-plane	PVA/H_2SO_4	1	2.3	3.05	0.3	60	69
				FS-IL	2.5	N/A	2.35	2	150	
CO_2 laser	Hydrated GO film	Free-standing	In-plane	Hydrated GO	1	0.51	3.1	0.43	1.7	20
CO_2 laser	PI	Free-standing	In-plane	H_2SO_4	1	4	1.5	0.3	50	47
				BMIM-BF_4	3.5	2	0.8	1	100	
fs 1030 nm laser	GO/$HAuCl_4$	Paper	In-plane	PVA/H_2SO_4	1	0.77	17.2	N/A	N/A	70
CO_2 laser	H_3BO_3/PI	Free-standing	In-plane	PVA/H_2SO_4	1	16.5	NA	0.5	2	71
laser-scribing DVD burner	CNT/GO	PET	In-plane	PVA/H_3PO_4	1	N/A	3.1	0.84	1	72
CO_2 laser	PI	Free-standing	In-plane	PVA/H_2SO_4	209	N/A	1.43×10^{-6}	31.3	N/A	73
CO_2 laser	PI	Free-standing	Sandwich	PVA/H_2SO_4	1	9.11	N/A	3	2.5	33
CO_2 laser	GO film	Free-standing	In-plane	BMIM	2.5	270	N/A	100	100	74
CO_2 laser	PI-LSG +Ni-CAT MOF	Free-standing	In-plane	PVA/LiCl	1.4	15.2	N/A	4.1	7	34
CO_2 laser	PI-LSG +PANI	Free-standing	In-plane	PVA/H_2SO_4	0.8	361	47.5	1.1	1.511	75
	PI-LSG +MnO_2	Free-standing	In-plane	PVA/LiCl	1	934	93.4	3.2	0.298	
	PI-LSG +FeOOH/LSG +MnO_2	Free-standing	In-plane asymmetric	PVA/LiCl	1.8	21.9	5.4	2.4	2.891	
CO_2 laser	PI-LSG +Fe_3O_4/LSG	Free-standing	In-plane asymmetric	PVA/H_2SO_4	1	719.28	63.04	5.3	0.02648	76
1064 nm laser	PI	Free-standing	In-plane	PVA/LiCl	1	1	N/A	1	0.02	77
			Sandwich			34.77	10.21	1	0.005	
355 nm ns laser	GO/Ni	PET	In-plane	PVA/LiCl	1	3.9	0.693	5.7	3	78
800 nm fs laser	GO film	Silicon oxide	In-plane	PVA/H_2SO_4	0.5	6.3	105	70	10	79
800 nm fs laser	GO film	PDMS	In-plane 3D	FS-IL	2.5	0.181	0.086	100	2200	80

GO: graphene oxide; PI: polyimide; PET: polyethylene terephthalate; PDMS: polydimethylsiloxane; fs: femtosecond; ns: nanosecond; CNTs: carbon nanotubes; PVA: poly(vinyl alcohol); BMIM-BF_4: 1-butyl-3-methylimidazolium tetrafluoroborate; $TEABF_4$: tetraethylammonium tetrafluoroborate; FS-IL: fumed silica nanopowder with the IL 1-butyl-3-methylimidazolium bis(trifluoromethyl sulfonyl)imide; BMIM: 1-butyl-3-methyimidazolium bis (trifluoromethyl sulfonyl) imide; Ni-CAT MOF: Ni-catecholate-based metal–organic frameworks; MnO_2: manganese dioxide; FeOOH: ferric oxyhydroxide; PANI: polyaniline;

ance) and contributes to an enhanced capacitance[67]. The poor conductivity of pseudocapacitive materials limits the power density. Moreover, the material deterioration during the redox process shortens the cycle lives of devices. The porous LSG with good conductivity and chemical stability was considered as a good framework of pseudo-capacitors. The LSG has been widely studied to fabricate both EDLCs and pseudo-capacitors. The electrochemical performances of diverse LSG-based SCs in literature were listed in Table 1.

LSG based electrochemical double-layer capacitors

In 2012, EI-Kady et al., fabricated the LSG based EDLCs by employing a standard LightScribe DVD optical drive, as shown in Figure 3(a)[68]. The GO films were deposited on the disk and then treated with laser. The resulting LSG shows a high electrical conductivity (1738 $S{\cdot}m^{-1}$) and a specific surface area (1520 $m^2{\cdot}g^{-1}$). An ion porous separator was sandwiched between two identical LSG electrodes for SCs (total thickness < 100 μm). The fabricated LSG SCs exhibit a energy density of 1.36 $mWh{\cdot}cm^{-3}$ and a power density of ~20 $W{\cdot}cm^{-3}$. With the similar laser direct writing technology, this research group demonstrates a scalable fabrication of LSG in-plane supercapacitors, Figure 3(b)[69]. The GO irradiated by laser was converted into graphene and applied as the SC electrodes. The unirradiated GO served as the separator between the positive and negative interdigitated electrodes. More than 100 LSG SCs can be produced on a single disc in 30 minutes or less. These efficiently fabricated LSG supercapacitors exhibit an ultrahigh power of 200 $W{\cdot}cm^{-3}$ and an excellent cycling stability retaining 96% of the initial performance after 10,000 charge-discharge cycles. Gao et al. demonstrated laser reduction and patterning of hydrated GO films for all-carbon monolithic supercapacitors[20]. The LSG electrodes were fabricated for both in-plane and conventional sandwiched supercapacitor. The hydrated GO, which contains substantial amounts of trapped water serves as both the electrolyte and the electrode separator. The resulting LSG SCs show a good cyclic stability (30% drop in the capacitance after 10,000 cycles) and a high areal capacitance (0.51 $mF{\cdot}cm^{-2}$). By laser scribing, the amorphous carbon nanospheres (CNS) precursors are transformed into highly turbostratic graphitic carbon (CNS-LSG)[81]. The sandwiched supercapacitors based on the CNS-LSG electrodes exhibit a high volumetric power density of 28 $W{\cdot}cm^{-3}$. For high quality LSG SCs, a CO_2 laser beam was employed to fabricate LSG with high crystallinity and a low degree of defects. Then a successive ultraviolet (UV)

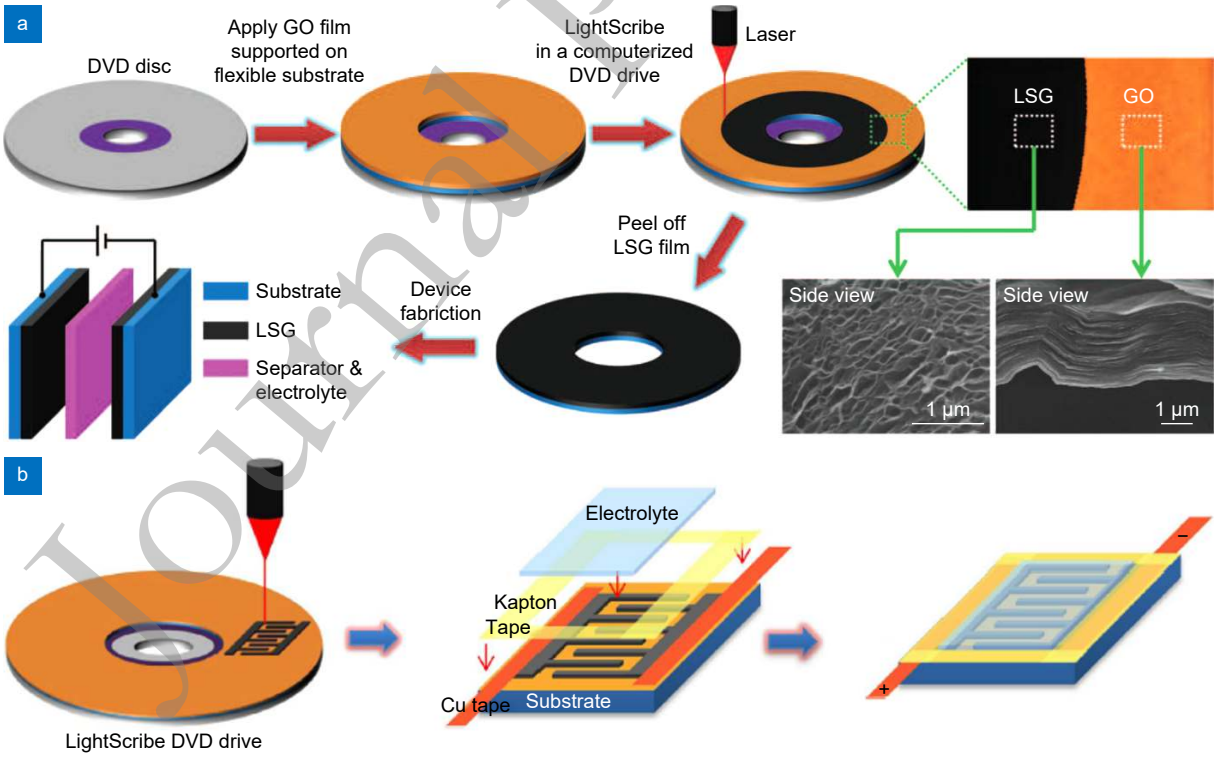

Fig. 3 | (**a**) Schematic illustration of the fabrication of LSG based supercapacitors with sandwiched structures[68]. (**b**) Schematic diagram of the preparation process for an in-plane LSG supercapacitor[69].

pulsed laser direct carving was performed for high resolution electrode pattern[82]. The fabricated SCs with an electrode width of 50 μm exhibit a areal capacitance of 43.7 mF·cm^{-2} and a 90% capacitance retention after 3000 cycles. In addition to the laser irradiation method, a successive electrochemical reduction was combined to fabricate highly conductive graphene networks for current collectors of supercapacitors[83]. The developed LSG supercapacitor shows notable improvement of the stability performances (100,000 cycles). A large cell voltage of 10.8 V was realized by modularizing nine devices in series, exhibiting rectangular shapes of the cyclic voltammetry curves at high scan rates of 100 V·s^{-1}.

Doped LSG for supercapacitors

Doping with heteroatoms (such as boron, nitrogen, phosphorus, and sulfur) has been regarded as an effective way to tailor the electrochemical properties of graphene-derived materials and to enhance their capacitive performances[84–86]. Heteroatom-doped graphene materials were intensely studied as active electrodes in energy storage devices. Tour et al., demonstrate that boron-doped porous graphene can be prepared from boric acid containing polyimide sheets using a facile laser induction process in ambient air, as shown in Figure 4(a)[71]. At the same time, the LSG was patterned for electrodes of flexible supercapacitors. Figure 4(b) shows that the B 1s peak of X-ray photoelectron spectroscopy (XPS) shifts from 192.5 eV in B-PI down to 191.9 eV in B-LSG after laser induction, showing the effective boron doping in the LSG sheet. The boron-doped LSG supercapacitor demonstrates an enhanced performance compared to bare LSG supercapacitor, as shown in Figure 4(c-d). The areal capacitance of boron doped LSG supercapacitor can reach 16.5 mF·cm^{-2}, 3 times higher than nondoped devices, with a concomitant energy density increase of 5-10 times. Fu et al., prepared N-doped LSG by direct laser writing on the mixture of the nitrogen-rich carbon nanoparticles and GO[87]. After laser treatment, the composites show N concentration as high as 7.78 atom %. With the N-doped LSG electrodes, the fabricated supercapacitors show a high capacity retention of 48.76% (18.17% for undoped LSG-SCs) at scan rate from 5 to 100 mV·s^{-1}. Similarly, Wang et al., synthesized nitrogen-doped and hierarchical porous graphene from GO/urea mixture using a picosecond laser[88]. This N-doped LSG SC reaches to a high areal capacitance of 60.7 mF·cm^{-2}, which is about 3 times higher than that of the undoped LSG SC. Instead of mixing in solution, Liu et al., treated KOH-coated polyimide films for synchronous heteroatoms (nitrogen and oxygen) doping and a wettability improvement of graphene by direct laser writing[89]. The nitrogen content can reach 4.94% and the doped LSG in-plane supercapacitors present an areal capacitance of 32 mF·cm^{-2} (4.27 μWh·cm^{-2}), which is about 10 times higher than that of the bare LSG.

Intercalated LSG for supercapacitors

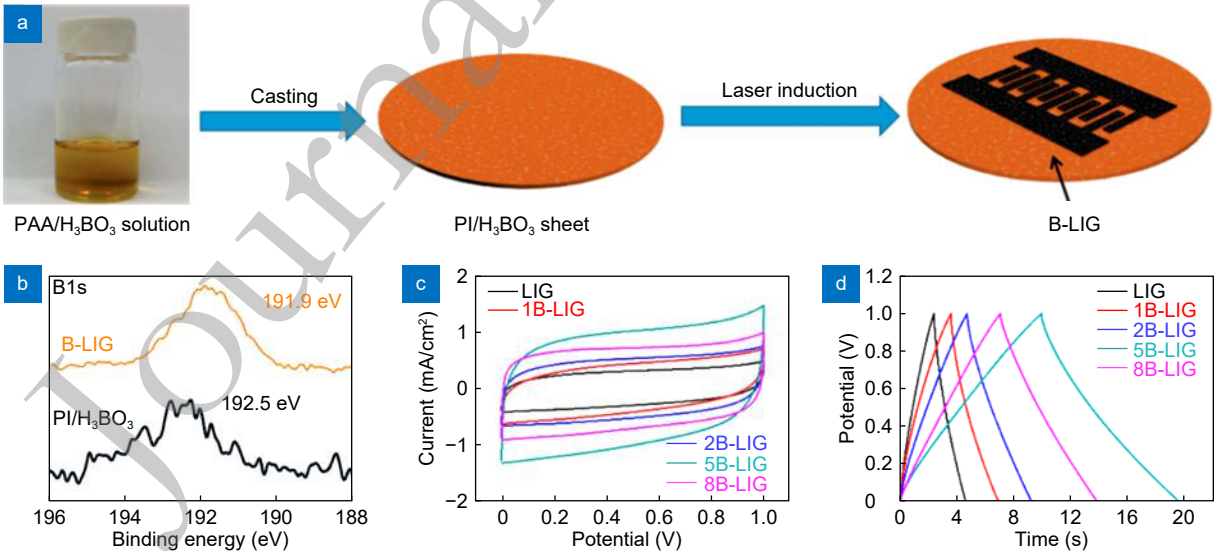

Fig. 4 | (**a**) Synthetic scheme for the preparation of boron-doped LSG and its fabrication of supercapacitor. (**b**) The B 1s spectrum of XPS spectra of PI/H_3BO_3 sheet and boron-doped LSG. (**c-d**) Cyclic voltammetry curves (c) and galvanostatic charge-discharge curves (d) of LSG SC and boron-doped LSG SC with different H_3BO_3 loadings[71].

Owing to the intensive pi –pi interaction of graphene, graphene sheets exhibit the strong tendency to restack together. The restacking issue leads to a significant decrease of ion-accessible surface area and thus a low capacitance of the graphene-based SC[90]. To prevent the restacking of LSG layers, carbon nanotubes (CNTs) with a smaller diameter (1-2 nm) were employed to insert between GO sheets before laser treatment, as shown in Figure 5(a)[72]. The GO/CNTs hybrid material was patterned into LSG/CNTs supercapacitors, yielding increased ion-accessible surface area. Figure 5(b-d) presents the images of LSG/CNT supercapacitor and the improved electrochemical performances. The laser-scribed LSG/CNT SC exhibits a volumetric capacitance of 3.10 F·cm^{-3}, a volumetric energy density of 0.84 mWh·cm^{-3} and a power density of 1.0 W·cm^{-3}. The SC retains 88.6% of the initial capacitance value after 5000 cycles. Similarly, ZnO nanoparticles with sizes ranging from 20 to 50 nm were inserted into the LSG sheets by laser scribing on the mixture of $Zn(NO_3)_2$ $6H_2O$ and GO[91]. Consequently, a 12 times improvement in the specific capacitance was achieved, compared with that of the pristine LSG SC. Lee et al., demonstrated that a tiny amount of Zn infiltrated into GO leaded to an explosive reduction of GO under laser irradiation[92]. Attributed to a larger specific surface area and lots of mesopores, the LSG/Zn SC exhibited a nearly 4 times increase in the energy density. Besides intercalated graphene, components with advanced properties were also combined with LSG for enhanced performances. Li et al., reduced the mixture GO and chloroauric acid ($HAuCl_4$) nanocomposite with a laser irradiation, patterning of LSG electrodes and producing Au nanoparticles in a one-step process, as shown in Figure 5(f-i)[70]. The porous LSG/Au electrode demonstrates a high conductivity of 1.1×10^6 S·m^{-1} and an enhanced accessible surface area. The LSG/Au SC shows an maximum specific capacitance of 3.84 mF·cm^{-2}. Sun et al., reported a laser fabrication of flexible planar supercapacitors from GO and black phosphorus quantum dots (BPQDs) nanocomposites[93]. The introduction of BPQDs with more active sites on GO edge boosted the ion transportation on the interface between the electrode and the electrolyte. The LSG-BPQDs based supercapacitor delivered an enhanced areal capacitance of 5.63 mF·cm^{-2} (1.87 mF·cm^{-2} for LSG). Li et al., deposited the LSG by the fabrication of polyimide onto 3D nickel foam, as a porous electrode with laser processing[94]. The LSG/Ni electrode shows a

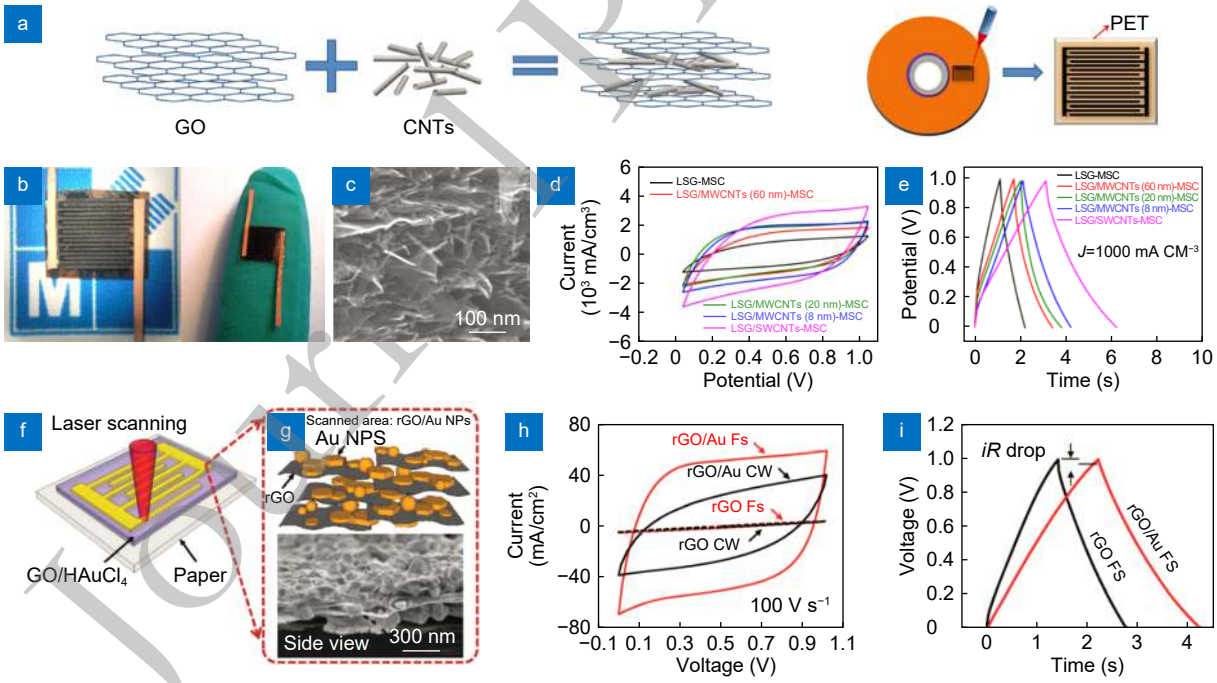

Fig. 5 | (**a**) Schematic showing the insertion of CNTs between GO layers to effectively inhibit the restacking and the fabrication process for the flexible supercapacitor (LSG/CNTs SC). (**b**) Digital photographs of an assembled SC. (**d-e**) Cyclic voltammetry curves (d), charge-discharge curves (e) and for LSG SCs, LSG/CNTs SCs with different diameters[72]. (**f**) Schematic illustration and photos of fabrication of LSG/Au supercapacitors onto a paper substrate. (**g**) The SEM image of LSG/Au microelectrodes. (**h-i**) Comparison of electrochemical performances of both the LSG/Au SCs and LSG SCs: cyclic voltammetry curves (h) and galvanostatic charge/discharge curves (i)[70].

high electrical conductivity (359,712 $S \cdot m^{-1}$) and the fabricated LSG/Ni supercapacitor demonstrated a large areal specific capacitance (995 $mF \cdot cm^{-2}$), a power densitiy (9.39 $mW \cdot cm^{-2}$) and over 98% capacitance retention after 10,000 cycles.

Pattern and structure of LSG based supercapacitors

Besides the electrode materials, the structure design of SCs has been also intensively studied to further enhance the performance of devices. Li et al., fabricated a flexible high-voltage LSG-SCs ranging from a few to thousands of volts with a planar in-series architecture, shown in Figure 6(a).[73] 210 isolated porous LIG squares were firstly patterned on PI by a programmable CO_2 laser system. The electrolyte was then added by brush coating process. The 209 V SC could achieve a high capacitance of 0.43 μF at a low applied current of 0.2 μA, and a capacitance of 0.18 μF at a high applied current of 5.0 μA. Figure 6(b) shows that a new structural design inspired by the traditional Japanese paper-cutting craftwork (known as "Kirigami"), has been employed to manufacture highly deformable SCs by laser-assisted graphitic conversion and cutting.[95] There is less than 2% shift in the LSG capacitance when the device is elongated to 382.5% of its initial length.[97] Figure 6(c) shows that vertically stacked LSG supercapacitors were assemblyed to multiply its electrochemical performance by laser induction on both sides of PI sheets.[33] A solid-state polymeric electrolyte, poly(vinyl alcohol) (PVA) in H_2SO_4 was applied for the assemblying of stacked LSG SCs. A novel bamboo-like series of in-fiber graphene supercapacitor was made along the GO fiber with LSG electrode arrays alternated with GO regions, as shown in Figure 6(d)[96]. Thousands of supercapacitor units can be fabricated within minutes and reach a high capacitance of 14.3

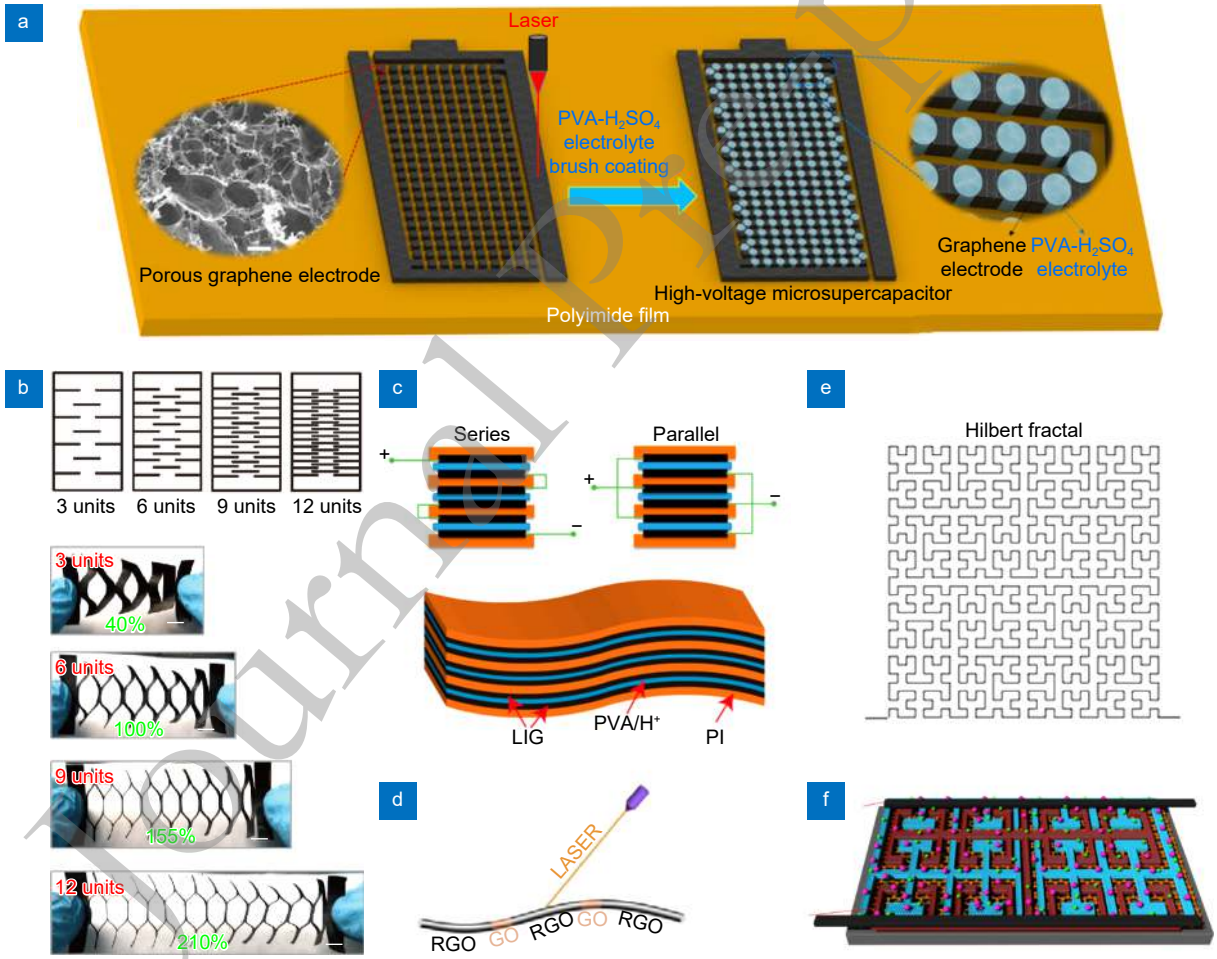

Fig. 6 | (**a**) Schematic diagram of a high-voltage planar SC based on laser scribed graphene[73]. (**b**) Schematic illustration and the related strain property of the kirigami-inspired electrodes with different geometric unit numbers (scale bar 1 cm)[95]. (**c**) Illustration of stacked LSG-SCs in series and parallel circuits and its structure[33]. (**d**) Schematic diagram of the direct laser reduction of GO fiber for the bamboo-like series of GO-LSG fiber[96]. (**e**) Bio-inspired fractal electrode design of Hilbert fractal structures. (**f**) Schematic structure of the Hilbert fractal electrode supercapacitor[74].

mF·cm^{-2}. Gu et al., designed new bio-inspired LSG electrodes including Hilbert fractal structures, Peano fractal structures and Sierpinski fractal structures, and thus compared the SC performances base on the different designs[74]. Electrodes with Hilbert fractal structures and the corresponding SC were demonstrated in Figure 6(e-f). Compared to the conventional planar supercapacitors, the Hilbert fractal designed SC increased the ratio of active surface area to volume of the electrodes and reduced the electrolyte ionic path. The energy density is thus significantly increased to ~10^{-1} Wh·cm^{-3}, more than 30 times higher than that achievable by the planar interdigital electrodes.

LSG based pseudo-capacitors

Compared to the EDLCs, pseudo-capacitors can achieve much higher capacitances since they store energy through a Faradic process, involving fast and reversible redox reactions between electrolytes and electro-active materials on electrode surfaces[67]. Transition metal oxides, hydroxides and conducting polymers are usually used as the electrodes for pseudo-capacitors[98]. However, owing to the poor electrical conductivity and the unstable structure of materials during the redox process, pseudo-capacitors demonstrate relatively low power densities and cycling unstabilities, which hinder their practical applications[65]. To overcome these drawbacks, graphene materials with high electrical conductivity and large specific surface area are merged with these active materials for pseudo-capacitor electrodes. Wu et al. combined a laser scribing technique with a subsequent low-temperature solvothermal growth of pseudo-capacitive materials to fabricate symmetric SCs with significantly improved electrochemical behaviour, as shown in Figure 7(a-c)[34]. A CO_2 laser beam was firstly used to convert the PI into porous LIG with an interdigitated architecture.

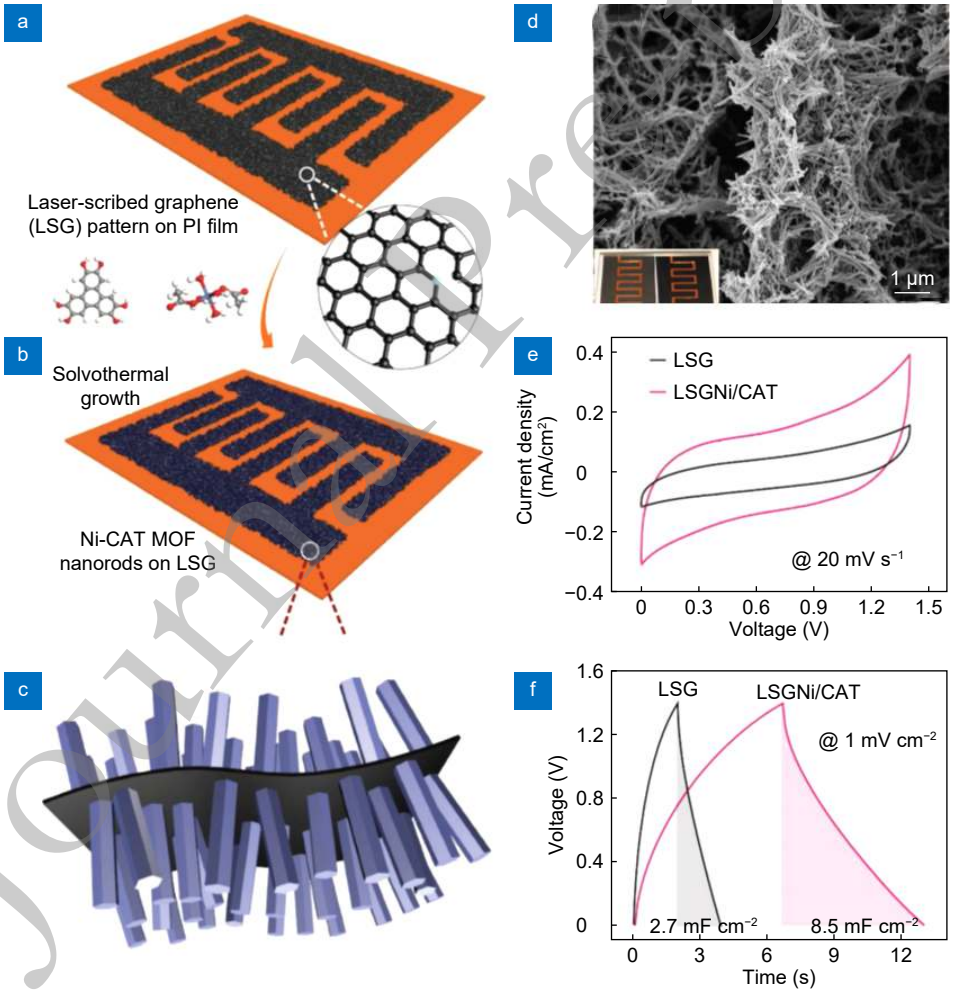

Fig. 7 | Schematic and structural illustration of LSG/Ni-CAT MOF. (**a**) An in-plane interdigital LSG pattern. (**b**) Solvothermal growth of Ni-CAT MOF nanorods. (**c**) Structure of LSG/Ni-CAT MOF. (**d**) SEM images of LSG and LSG/Ni-CAT MOFs, respectively. (**e**) Cyclic voltammetry comparison of bare LSG and LSG/Ni-CAT MOF. (**f**) Galvanostatic charge/discharge curves of bare LSG and LSG/Ni-CAT MOF[34].

Then, the conductive Ni-catecholate-based metal-organic frameworks (Ni-CAT MOF) were selectively grown on 3D LSG with a low-temperature solvothermal method. Figure 7(d) depicts that the tiny uniform nanorods are anchored on the LSG sheets and the black-grey pattern turns into dark blue (inset of Figure 7(d)). Figure 7(e-f) demonstrates the cyclic voltammetry (CV) curves and the galvanostatic charge/discharge (GCD) curve of the bare LSG electrode and that of the LSG/Ni-CAT composite. The SCs with LSG/Ni-CAT MOF electrodes exhibit a wide operating voltage (1.4 V), a high areal capacitance (15.2 mF·cm^{-2}), a high energy density (4.1 μWh·cm^{-2}), a high power density (7 mW·cm^{-2}), and a capacitance retaining of 87% after 5000 cycles. With electrodeposition method, Tour et al. reported that manganese dioxide (MnO_2), ferric oxyhydroxide (FeOOH) or polyaniline (PANI), was deposited onto the LSG forming LSG –MnO_2, LSG –FeOOH, and LSG –PANI composites for SCs[75]. Both the symmetric SCs of LSG –MnO_2 and LSG –PANI, and asymmetric SCs of LSG –FeOOH/LSG –MnO_2 were fabricated. For the LSG –MnO_2 SCs, the energy densities can reach 32.4 μWh·cm^{-2} and 3.2 mWh·cm^{-3}, which is an increase of > 1200 and > 290 times, respectively, compared with that of LSG SC. For LSG–PANI SCs, the energy densities are 8.0 μWh·cm $^{-2}$ and 1.1 mWh·cm $^{-3}$, which are 41 and 15 times higher, respectively, than that of LSG SC. The ferrocene was also chemically bonded to the LSG by vapor deposition or wet adsorption. The graphene/ferrocene pseudo-capacitors was fabricated with an energy density of 6.19 Wh·kg^{-1} while maintaining a power density of 26.0 kW·kg^{-1}[99]. Yang et al., synthesized the Co_3O_4 nanoparticles/graphene composites by irradiating the mixed solution of porous Co_3O_4 nanorods and GO with laser[100]. The Co_3O_4/graphene supercapacitor reaches a high specific capacitance of 978.1 F·g^{-1} (135.8 mAh·g^{-1}) at the current densities of 1 A·g^{-1}. It also shows a more than 93.7% capacitance retention at the current density up to 10 A·g^{-1} with 20,000 cycles. In another report, the bisterpyridyl based molecular cobalt complexes (TPy-Co) inks were inkjet-printed onto the surface of LSG as pseudocapacitive additives[101]. The specific capacitance of the fabricated pseudo-supercapacitor was increased by 75 times without sacrificing the charging and discharging rates. The oxygen-deficient TiO_2/LSG (OD-TiO_2/LSG) was prepared with a laser irradiation on mixed solution of TiO_2 nanocrystals and GO[102]. The ODTiO_2/LSG supercapacitor delivered a maximum energy density of 14.1 Wh·kg^{-1} and a maximum power density of 8.5 kW·kg^{-1}. Moreover, polyaniline nanofibers were electrodeposited on LSG for extended surface area of the electrode, pseudocapacitance and prevention of the graphene restacking[103]. The composite electrode presents a specific capacitance of 442 F·g^{-1} and a capacitance retention of 84% over 2000 cycles. The polymerized poly (3,4-ethylenedioxythiophene) (PEDOT) was spin-coated on the surface of LSG for SC application, with enhanced pathways for charge transport and the conductivity of the component films[104]. The fabricated supercapacitors displayed reversible capacities of 115.2, 97.0, and 78.4 F·g^{-1} at rates of 0.5, 2, and 6 A·g^{-1}, respectively.

LSG based hybrid supercapacitor

To maximize the benefits of existing supercapacitors (high power density and stable cycle performance) and lithium-ion batteries (high energy density), hybrid supercapacitors were proposed by Naoi in 2009 by using an asymmetric electrode[105,106]. Asymmetric supercapacitors have been extensively explored by combining Faradic electrodes and capacitive electrodes to enhance energy density of high-power SCs[107]. Liu et al., reported a facile fabrication of an in-plane hybrid supercapacitor with the Fe_3O_4 nanoparticle-anchored LSG (LSG/Fe_3O_4) as the anode and LSG as the cathode[76]. Figure 8(a) demonstrates the preparation of LSG/Fe_3O_4 with laser irradiation on $FeCl_3$ crystal-coated PI film and subsequent laser annealing. Figure 8(b-c) shows the 3D porous LSG was well wrapped by the Fe_3O_4 nanoparticles. Figure 8(d-e) demonstrates that the LSG/Fe_3O_4 exhibits an enhanced performance compared to that of LSG, due to the Faradaic redox reaction of the electrochemically active Fe_3O_4 nanoparticles. This hybrid supercapacitor demonstrates an ultrahigh areal capacitance of 719.28 mF·cm^{-2} and an areal energy density of 60.2 μWh·cm^{-2}. The superior performance is attributed to both the reversible H^+ ion (de) intercalation reaction with Fe_3O_4 nanoparticles, significantly increasing the energy density and the unique 3D structures in LIG/Fe_3O_4, leading to super hydrophilic and capillary effects. Lee et al., designed novel compositions of LSG cathodes and $AlPO_4$-carbon hybrid coated $H_2Ti_{12}O_{25}$ (H-HTO) anodes for coin-type hybrid supercapacitors.[108] The LSG/H-HTO combination exhibits asuperior electrochemical activity with energy densities of 17.7 –70.8 Wh·kg^{-1}, power densities of 195.1 –5191.9 W·kg^{-1}, a cycling stability of 98% after

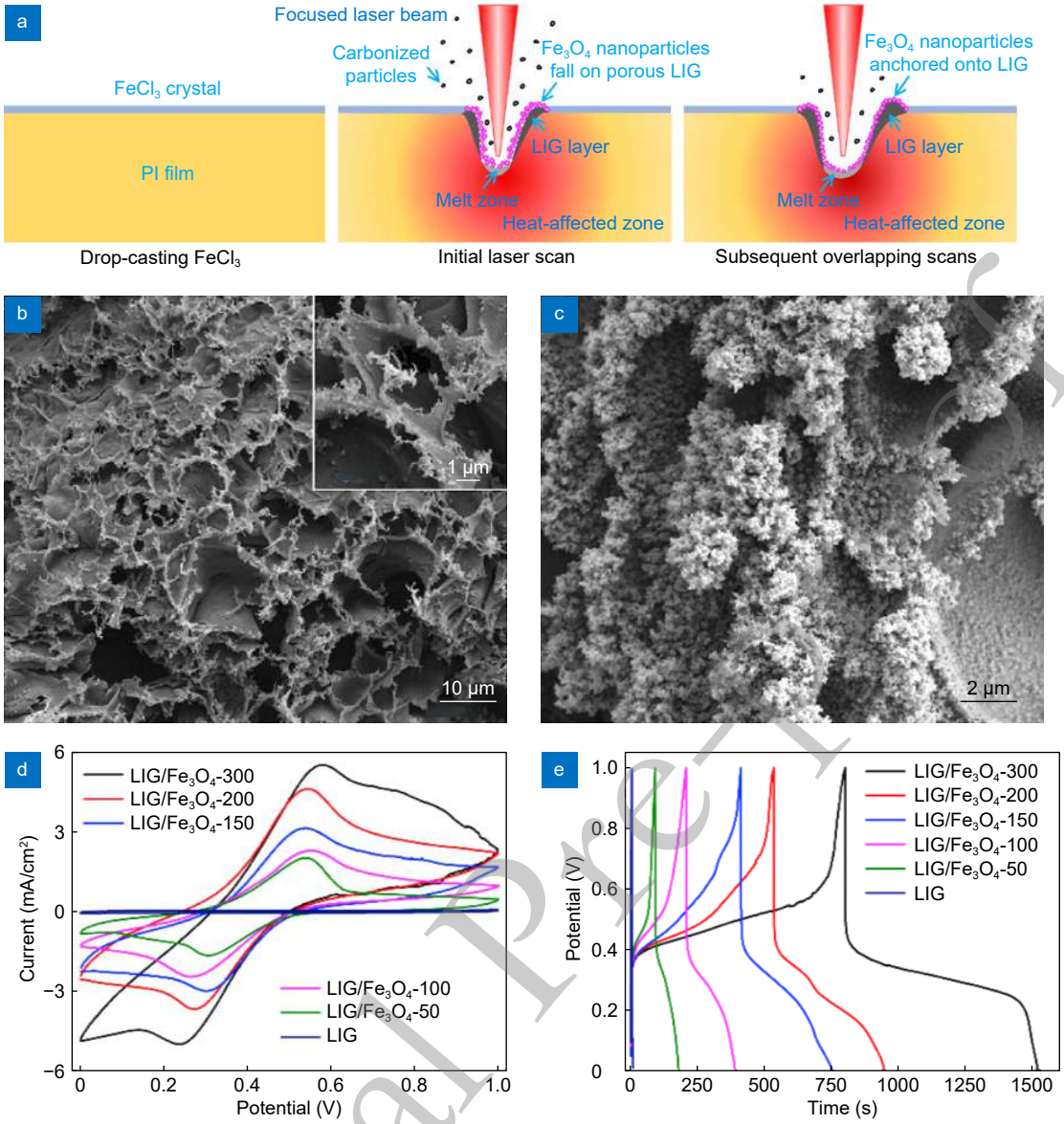

Fig. 8 | (**a**) Schematic illustration of the deposition process of laser-oxidized Fe_3O_4 nanoparticles anchored on porous laser scribed graphene by direct laser writing technique. (b-c) SEM images of (**b**) 3D porous LSG and (**c**) 3D LSG/Fe_3O_4 nanoparticle composite. (**d**) CV curves of LSG/Fe_3O_4-X at 5 mV·s^{-1} (**e**) GCD profiles of LSG/Fe_3O_4-X at 1 mA·cm^{-2}[76].

10000 cycles and a rate capability of 78% at a high current density of 3.0 A·g^{-1}. A facile solution mixing and a subsequent laser reduction method were reported to fabricate LSG/$LiNi_{1/3}Mn_{1/3}Co_{1/3}O_2$ (LSG/NMC) composite for high energy cathode materials in hybrid supercapacitors[109]. The LSG/NMC composites demosntrate a high capacitance of 141.5 F·g^{-1} and an excellent capacitance retention of 98.1% after 1000 cycles. Beside asymmetric electrodes, MoS_2 decorated LSG (MoS_2/LSG) was fabricated for hybrid supercapacitors by direct laser writing on PI coated with MoS_2 flakes[110]. The graphitization of PI and the MoS_2 decoration of the obtained LSG were achieved by one-step laser treatment. The porous LSG facilites the effective transportation of electrolyte ions and electrons throughout the electrode network, resulting in doublelayer capacitances. The decorated MoS_2 contributes to the pseudocapacitance, originating from faradaic charge-transfer mechanism. This combination of pseudo and double-layer capacitances enables the comprehensive MoS_2/LSG SCs with excellent electrochemical performances. Moreover, Liu et al. employed lithium containing polymer gel electrolyte for LSG supercapacitors fabricated via a direct semiconductor laser writing on PI sheets[77]. The LSG supercapacitors exhibit high areal specific capacitance up to 34.7 mF·cm^{-2}, while that with the acid gel electrolyte is 8 mF·cm^{-2}. This sub-

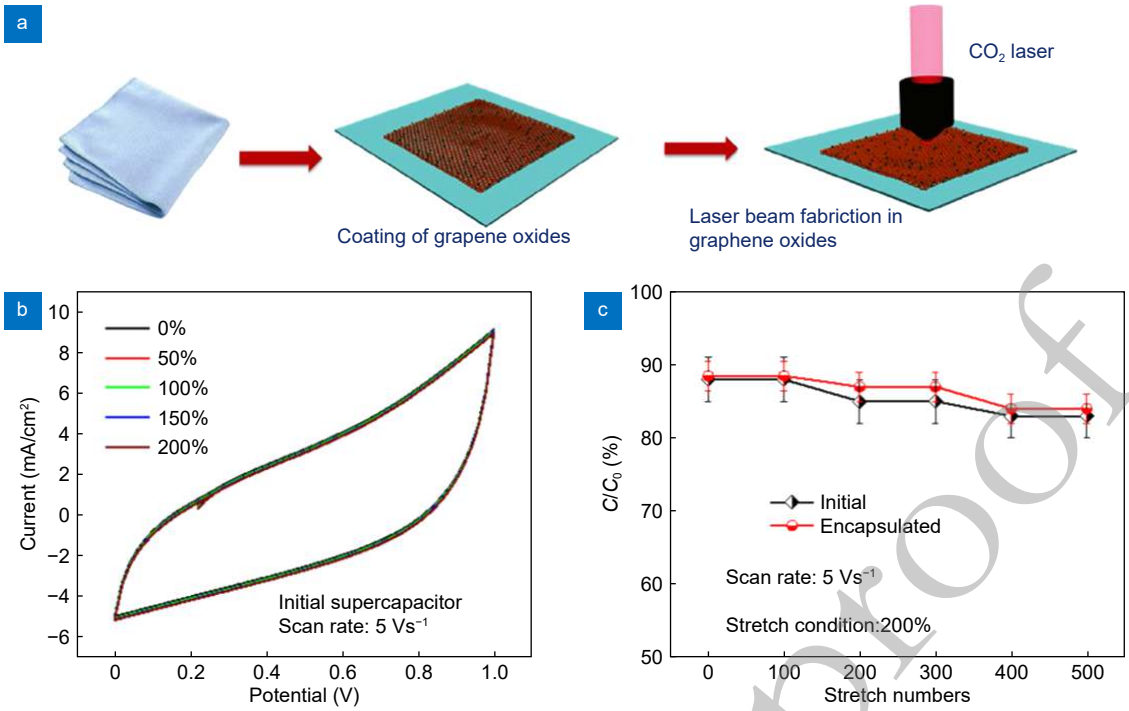

Fig. 9 | (**a**) Schematic of the fabrication steps for the LSG supercapacitor on textile. (**b**) CV measurements on LSG supercapacitors without encapsulation under different stretchable conditions for a scan rate of 5 V·s^{-1}. (**c**) Capacitance retention under the maximum stretchable condition of 200% along the uniaxial direction for a scan rate of 5 V·s^{-1}[111].

stantial enhancement is considered to be due to the combination of Faradaic intercalation and non-Faradaic absorption of the Li-ions at the LSG electrodes.

Featured LSG supercapacitor

Flexible LSG supercapacitor

With the increasing development of wearable devices, flexible energy storage unites are highly demanded. Gu et al., reported large-scale flexible LSG supercapacitors with dimension 100 cm^2 fabricated on textiles in 3 minutes as shown in Figure 9(a)[111]. The fabrics were paint-coated with the GO/Matte binder solution to form thin films with thicknesses of 3 μm, which were then treated with a CO_2 laser. The fabricated SCs demonstrate an excellent water stability, an areal capacitance of 49 mF·cm^{-2}, an energy density of 6.73 mWh·cm^{-2} and a power density of 2.5 mW·cm^{-2}. The LSG SCs show stable CV results for a maximum of 200% stretchability and a high capacitance retention of 88% under 500 cycles of 200% stretching condition, as shown in Figure 9(b-c). Xie et al., presented LSG SCs on the flexible substrate of Poly(ethylene terephthalate) (PET, 6 μm-thick)[78]. With electrostatic spray deposition method, the uniform GO film was deposited on a PET covered with Ni film (500 nm). By adjusting the laser power, the reduction and patterning of LSG electrode arrays can be fabricated in just one batch. These ultrathin (18 μm) SCs show a negligible change in the CV curves under 0 –180° bending, suggesting their excellent flexibility. These flexible LSG SCs demonstrate high performances of out-standing scan rate (1000 mV·s^{-1}), including an excellent cycle stability (20,000 cycles) and a high volumetric energy density (0.98 mWh·cm^{-3} in PVA/LiCl aqueous gel 5,7 mWh·cm^{-3} in ionic liquid). To provide good mechanical properties for the stretchable devices, Lamberti et al., transferred porous LSG to elastomeric polydimethylsiloxane (PDMS) by vacuum infiltration and thermal curing[112]. The LSG/PMDS electrodes were then assembled and sealed into the sandwiched supercapacitors, which show good retention of energy storage performances under bending and stretching conditions. The CVs of the fabricated LSG/PDMS device remains almost unchanged even at the high scan rate of 10 V·s^{-1} during the stretching of 0–50% and bending process of 0°–160°. The devices also show an excellent cycling stability, retaining 84% of their initial capacitance after 1000 cycles in stretching condition and almost 90% in the bending condition. Furthermore, a PDMS/PI powder composite was directly treated by a CO_2 laser, resulting in the graphitization of polyimide for the application of flexible strain gauge and supercapacitor[113]. The laser-written PDMS/PI substrates are

sufficiently electrically conductive and mechanically stable for flexible electronics. A flexible melamine foam was employed as the skeleton to attach the GO sheets[114]. After laser irradiation, the sandwiched LSG -GO -LSG foam supercapacitor shows a high capacitance performance which can be easily regulated by adjusting the compressive state of electrodes. The supercapacitors show a volumetric energy density of 0.04 mWh·cm^{-3} and 1 mWh·cm^{-3} under 0% and 90% strain, respectively.

Miniaturized LSG supercapacitor

The large dimension of LSG significantly limits the density of graphene electrodes of the supercapacitor, decreases the effective surface area and thus severely deteriorates the energy densities of supercapacitors[116]. Consequently, the fabrication of LSG with a high spatial resolution is a promising approach to enhance energy densities of supercapacitors. Due to the diffraction limit and the heat diffusion generated during the laser reduction, the linewidth of LSG electrodes in a supercapacitor is strongly related to the laser direct writing system[115]. The fs laser fabrication is mainly considered as a non-thermal fabrication process, which involves the multiphoton absorption within the time scales of less than a picosecond[18]. By avoiding the undesired heat diffusion, this fabrication method can lead to high-resolution structures. Kumar et al., fabricated graphene-based in-plane micro-supercapacitor (MSCs) devices with 100 μm width electrodes and a spacing of 400 μm between electrodes by 355 nm ns laser direct writing onto free-standing GO films (thickness 2.2 μm)[117]. The fabricated MSCs with liquid electrolyte have a capacitance of 288.7 mF·cm^{-3} and a good cycling stability. Similarly, In et al., fabricated flexible LSG MSCs with the electrode width of 120 μm and the gap distance of 90 μm with 522 nm fs laser direct irradiation on PI sheets. The areal capacitance of the fabricated SCs reaches 800 μF·cm^{-2} at a voltage scan rate of 10 mV·s^{-1}[118]. Tour et al. used visible 405 nm laser to directly convert PI into LSG with a spatial resolution of ~12 μm and a thickness of < 5 μm, as shown in Figure 10(a)[115]. Furthermore, Shen et al., produced ultraminiature MSC electrodes with 100 μm long, 8 μm wide and 2 μm spacing, based on fs laser reduced graphene oxide[79]. With fs laser-induced forward transfer, an electrolyte microdroplet was accurately transferred on top of each electrode, avoiding any interference of the electrolyte with other electronic components, as shown in Figure 10(b). Figure 10(c-d) shows the image of LSG electrodes for SCs. The CV curves of MSCs with electrodes width of 2 μm and 550 μm are compared in Figure 10(e-f), indicating that the miniaturization of MSC electrodes enhances the specific capacitance density. These MSCs exhibit a high specific capacitance (6.3 mF·cm^{-2} and 105 F·cm^{-3}) and ~100% retention after 1000 cycles. In addition, multi-layer 3D stacked MSCs based on laser carbonization of polyimide (PI) sheets were achieved with 3D femtosecond laser direct writing techniques[119]. For the fabrication of 3 layers stacked SCs, fs laser is first focused at the 80 μm, then 60 μm and 0 μm below the surface of PI sheets. The total thicknesses of 2 layers and 3 layer MSC are around 115 μm and 140 μm, respectively. The 2-layer and 3-layer stacked MSCs show

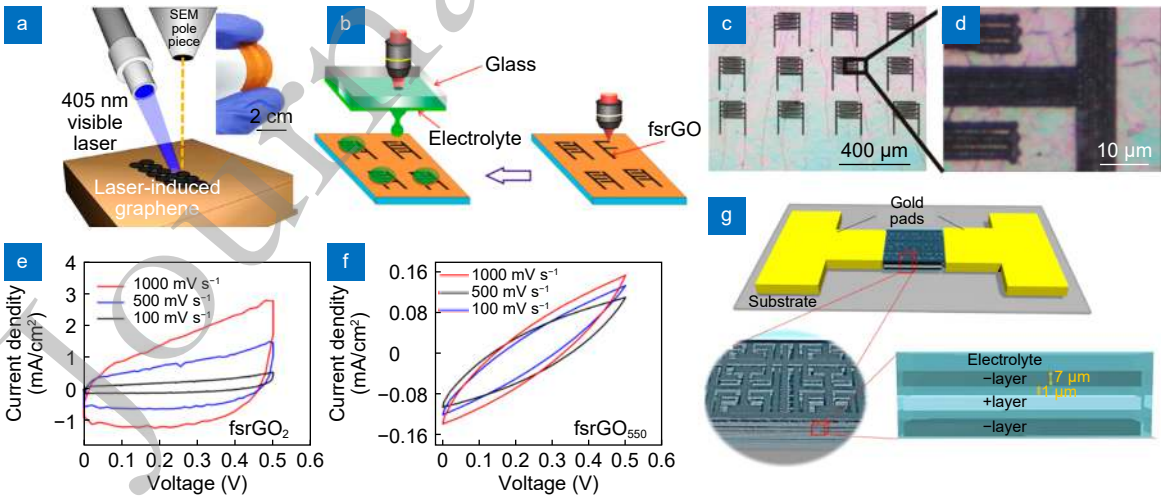

Fig. 10 | (**a**) Schematic of experimental setup using a 405 nm laser in SEM[115]. (**b**) Fabrication of integrated micro-supercapacitors on a GO film using fs laser processing. (**c-d**) LSG electrode arrays maintain high resolution with a spacing of ~2 μm. (**e-f**) CV profiles of fs MSC with the interelectrode spacing of (e) 2 μm and (f) 550 μm[79]. (**g**) Two-photon-induced 3D graphene micro-supercapacitor using a fs laser[80].

an improved areal capacitance as high as 37.2 mF·cm^{-2} and 42.6 mF·cm^{-2} at a current density of 0.1 mA cm^{-2}, respectively. With two-photon direct fs laser writing technology, Gu et al., developed high-performance 3D LSG MSCs with the fractal electrode distance down to 1 μm, as shown in Figure 10(g)[80]. The charge transfer capability enhanced by order of 10^2 and the fabricated SCs show an energy storage density of 10^{-1} Wh·cm^{-3} and a volumetric capacitance of 86 mF·cm^{-3} with stretchability of 150%. This performance enhancement is attributed to the growth of defects within the increase of layers. Yuan et al., reported a spatially shaped femtosecond laser (SSFL) method for patterning of LSG/MnO_2 SCs[120]. Different from previous laser direct writing method, the initial Gaussian beam were modulated to various beam shapes using phase modulations, which can pattern the LSG MSCs with designed shapes. It greatly enhances the fabrication efficiency and over 30,000 LSG MSCs can be produced within 10 minutes. The fabricated MSCs were dozens of microns with gaps of 500 nm and exhibit a high energy density (0.23 Wh·cm^{-3}) and outstanding specific capacitance (128 mF·cm^{-2} and 426.7 F·cm^{-3}).

Integrated LSG supercapacitor

With the recent rapid growth of portable and multifunctional electronic devices, the studies of integrated energy devices have attracted enormous attention. Gu et al. integrated the in-plane supercapacitors with commercial c-Si solar cells by using a CO_2 laser to scribe the GO film on the reverse side of solar cells, as shown in Figure 11(a)[121]. Under light illumination, electron-hole pairs are generated in the silicon solar cell and eventually collected by the LSG energy storage unit. The integrated devices lead to the miniaturization in size without sacrificing the performance. Similarly, Liu et al. combined a silicon solar cell with a LSG sandwiched supercapacitor for energy harvesting and energy storage individually[124]. Besides the energy unit, Watanabe et al. developed a self-powered UV light detection system with LSG SCs as energy storage units, shown in Figure 11(b-d)[122]. The LSG SC and a ZnO nanoparticles-based photodetector were prepared by a one-step laser direct writing process and were integrated with commercial solar panels. It was demonstrated that the SC can be easily charged within 1 minute by the solar panel and remain above 0.55 V

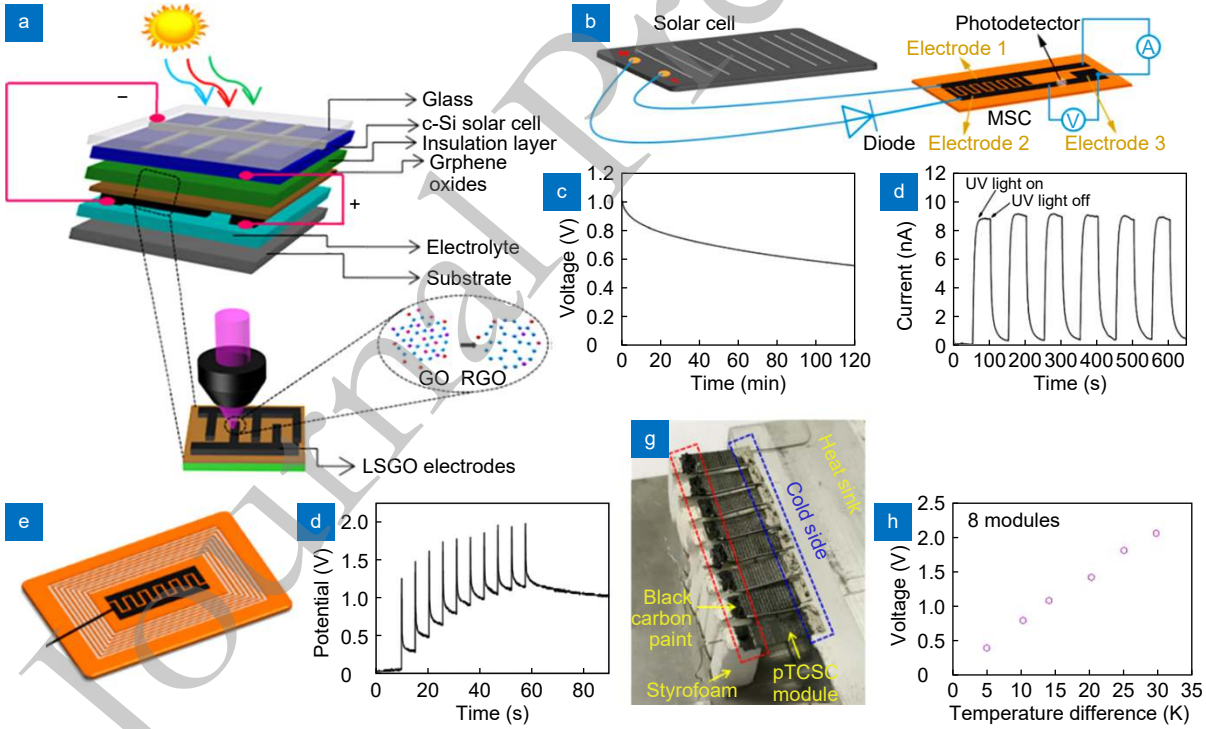

Fig. 11 | Schematic of the integrated energy storage with silicon solar cells[121]. (**b**) Schematic illustration of the self-powered photodetection system including a commercial solar panel, a SC, and a ZnO-based photodetector. (**c**) Self-discharge curve of the SC after being charged by the solar panel for 1 minute. (**d**) Photocurrent curves of the photodetector driven by the SC[122]. (**e**) Schematic illustration for the fabrication of a wireless charging and storage integrated device. (**f**) Potential change of the integrated SC charged by the wireless circuit placed on a commercial wireless charger[56]. (**g**) Serially connected thermally chargeable SC modules whose ends are colored in black and silvery-white to create temperature differences under solar radiation. (**h**) The steady-state voltage of 8 thermally chargeable SC modules as a function of ΔT[123].

after 2 h, which is sufficient to drive the UV photodetector. Based on the laser direct writing on a PI film, the same research group also combined micro-circuits for wireless charging with LSG SC for energy storage, Figure 11(e-f). This integrated device can be wirelessly charged by a commercial wireless charger[56]. Kim et al., reported a novel thermally chargeable supercapacitor that can convert thermal energy to electricity and then store charge simultaneously, Figure 10(g-h)[123]. These devices were fabricated with laser irradiation on GO films intercalated by sulfate ions. With a temperature gradient of 10.5 K, a thermally charged voltage of 58 mV can be generated. This supercapacitor can perform as long as a temperature gradient exist. Therefore, any heat dissipating objects including the human body and power-consuming devices can be utilized as power source for charging. This laser direct writing for graphene shows a facile and versatile process, can be compatible with various devices and indicates great potential for integrated multifunctional units.

Conclusions and Outlook

As concluded in this review, great progress has been made in the research field of LSG SCs. LSG can be fabricated from various precursors including GO, polymer and biomass with different laser systems. And its modifications were achieved by adjusting the laser parameters, fabrication processing and environment. The laser direct writing technology can simply induce graphene and simultaneously pattern the graphene electrodes for supercapacitors. Based on LSG, the fabrication of EDLCs, pseudo-capacitors and hybrid supercapacitors and their performances were discussed. Numerous studies have devoted to developing LSG SCs with enhanced performances by element doping, intercalation and pattern optimization. Diverse supercapacitors with advanced features such as being flexible, high power density, miniature, high voltage and new pattern design were also illustrated. The LSG SCs hold great potential for energy storage in the future.

However, there is still room for further improvements. Due to the increasing demand for the portable devices, the miniaturization of energy units is highly expected[125]. Currently, the resolution of laser direct writing, which is typically several micrometres or even millimetres has severally restricted the size of LSG SCs. Meanwhile, the number of LSG electrodes on devices was decreased due to the low resolution, which hampers the energy density of LSG SCs. It was highly expected to further improve the resolution of LSG for fabricating the nano-supercapacitors and enhancing their performances. For the fabrication of asymmetric SCs, the laser direct writing process is always followed with electrodeposition process to deposit the pseudo-capacitive materials on one of the electrodes of the in-plane supercapacitors. However, this process may not be suitable for the fabrication of asymmetric MSCs considering the size. Other leading methods or technologies, such as printing or lithography should be explored and combined with laser direct writing method.

Moreover, a broad range of precursors should be explored for LSG, considering not only the properties of LSG but also their impacts on environment and potential for massive production. Various carbon sources, which were traditionally considered as waste, could be reused as precursors of LSG fabrication. The development of potential precursors can effectively utilize resource, reduce pollution and promote the massive production of LSG. In addition, the integration of LSG SCs with energy-generating and energy-consuming components should be further developed. Various energy devices, including thermal or mechanical energy generator, can be investigated as future energy suppliers of LSG SCs. The energy-consuming devices including diverse LSG sensors and LSG transistors can also be integrated. Importantly, these integrated all-LSG devices entirely engraved by laser will facilitate scalable manufacture and the industrialization of LSG SCs. The integration of supercapacitors, solar cells and radiative coolers can also be very attractive. Radiative cooling is a promising cooling method without external energy consumption. The radiative coolers can simultaneously possess a high solar reflection up to 97% and strong infrared emission, cooling the object below ambient temperature[126,127]. The reflected solar can be redirected to solar cell for higher absorption efficiency. The decreased temperature can improve the efficiency of the integrated devices since the rising operation temperature deteriorates the performance and reliability of solar cells[128,129].

Furthermore, the laser technology should be combined with other advanced technologies. As a significant technique, artificial intelligence (AI) is emerging as an effective approach to solving complicated problems in various fields and is becoming more and more important nowadays[130,131]. AI system can adapt its parameters and generate desired outputs from given inputs. It has

been applied to emulate the human cognitions, including autonomous decision, deduction, adaption and interpretation[132]. In the research of LSG SCs, AI can be very favorable in several key sectors, including pattern designs, fabrications and applications. The AI-driven inverse design has demonstrated great potential in the demanded design of structures and devices[133,134]. Giving certain conditions and constraints, a sequence of patterns can be inversed designed by AI for modelling of the LSG SCs and prediction of their performances. Through the "training" phase, the unseen internal nonlinear relationships between the layout of electrodes and the performances of the corresponding LSG SCs can be statistically acquired. To meet the requirements of various applications, the LSG SCs can be custom-designed to achieve different energy densities, power densities and reliabilities. Avoiding conventional regulatory and constrains, AI offers tremendous potential for the novel patterning designs of LSG SCs. Meanwhile, the self-learning ability of AI gives it great advantage of biomimetic design. The bioinspired structures can largely enhance the variation of the electrode layout. With the assistance of the AI, diverse biomimetic designs for LSG SCs can be further optimized to improve the accessible active area of the electrodes and reduce the electrolyte ionic path. AI can also be utilized for accurate fabrication of LSG SCs. In the LSG production, laser spot sizes, laser powers, laser scan speeds strongly affect the reduction degree and the morphology of LSG, which largely determine the performance of fabricated LSG SCs. A variety of algorithms can be developed, combining AI with domain knowledge in laser parameters and properties of the resulting LSG. AI facilitates the production of LSG with targeted properties. Ultra-narrow LSG electrodes with accurately controlled gaps can be realized to reduce the size of devices and increase the density of electrodes. With the assistance of AI, 3D LSG SCs with complex configurations will also be precisely manufactured. AI can play a significant and decisive role to improve the fabrication capability of LSG SCs and achieve their desired performances. For the applications of LSG SCs, the implement of AI is very promising for developing intelligent energy management systems. With the properties of LSG SCs, energy production units and energy consuming components in the system, AI can forecast the power demanding, tune the output of individual device and balance the power supplies within the energy system. Especially for the highly integrated SCs systems, this overall predication and evaluation of the device performances can effectively enhance the efficiencies and reliabilities of the whole energy systems.

References

1. Zheng XR, Jia BH, Lin H, Qiu L, Li D et al. Highly efficient and ultra-broadband graphene oxide ultrathin lenses with three-dimensional subwavelength focusing. *Nat Commun* **6**, 8433 (2015).
2. Yun XW, Xiong ZY, Tu L, Bai LQ, Wang XG. Hierarchical porous graphene film: an ideal material for laser-carving fabrication of flexible micro-supercapacitors with high specific capacitance. *Carbon* **125**, 308–317 (2017).
3. Bellani S, Martín-García B, Oropesa-Nuñez R, Romano V, Najafi L et al. "Ion sliding" on graphene: a novel concept to boost supercapacitor performance. *Nanoscale Horiz* **4**, 1077–1091 (2019).
4. Wu MM, Li YR, Yao BW, Chen J, Li C et al. A high-performance current collector-free flexible in-plane micro-supercapacitor based on a highly conductive reduced graphene oxide film. *J Mater Chem A* **4**, 16213–16218 (2016).
5. Chen CM, Zhang Q, Yang MG, Huang CH, Yang YG et al. Structural evolution during annealing of thermally reduced graphene nanosheets for application in supercapacitors. *Carbon* **50**, 3572–3584 (2012).
6. Huang GW, Li N, Du Y, Feng QP, Xiao HM et al. Laser-printed in-plane micro-supercapacitors: from symmetric to asymmetric structure. *ACS Appl Mater Interfaces* **10**, 723–732 (2018).
7. Zhao B, Liu P, Jiang Y, Pan DY, Tao HH et al. Supercapacitor performances of thermally reduced graphene oxide. *J Power Sources* **198**, 423–427 (2012).
8. Chen YM, Guo MH, He L, Yang W, Xu L et al. Scalable microfabrication of three-dimensional porous interconnected graphene scaffolds with carbon spheres for high-performance all carbon-based micro-supercapacitors. *J Mater* **5**, 303–312 (2019).
9. Geim AK, Novoselov KS. The rise of graphene. *Nat Mater* **6**, 183–191 (2007).
10. Li GJ. Direct laser writing of graphene electrodes. *J Appl Phys* **127**, 010901 (2020).
11. Zhao Y, Han Q, Cheng ZH, Jiang L, Qu LT. Integrated graphene systems by laser irradiation for advanced devices. *Nano Today* **12**, 14–30 (2017).
12. Novoselov KS, Geim AK, Morozov SV, Jiang D, Zhang Y et al. Electric field effect in atomically thin carbon films. *Science* **306**, 666–669 (2004).
13. Bae S, Kim H, Lee Y, Xu XF, Park JS et al. Roll-to-roll production of 30-inch graphene films for transparent electrodes. *Nat Nanotech* **5**, 574–578 (2010).
14. Wang SJ, Geng Y, Zheng QB, Kim JK. Fabrication of highly conducting and transparent graphene films. *Carbon* **48**, 1815–1823 (2010).
15. Wan ZF, Streed EW, Lobino M, Wang SJ, Sang RT et al. Laser-reduced graphene: synthesis, properties, and applications. *Adv Mater Technol* **3**, 1700315 (2018).
16. Bergsman DS, Getachew BA, Cooper CB, Grossman JC. Preserving nanoscale features in polymers during laser in-

duced graphene formation using sequential infiltration synthesis. *Nat Commun* **11**, 3636 (2020).
17. Guo L, Jiang HB, Shao RQ, Zhang YL, Xie SY et al. Two-beam-laser interference mediated reduction, patterning and nanostructuring of graphene oxide for the production of a flexible humidity sensing device. *Carbon* **50**, 1667–1673 (2012).
18. Li XP, Ren HR, Chen X, Liu J, Li Q et al. Athermally photoreduced graphene oxides for three-dimensional holographic images. *Nat Commun* **6**, 6984 (2015).
19. Loeian MS, Aghaei SM, Farhadi F, Rai V, Yang HW et al. Liquid biopsy using the nanotube-ctc-chip: capture of invasive ctcs with high purity using preferential adherence in breast cancer patients. *Lab Chip* **19**, 1899–1915 (2019).
20. Gao W, Singh N, Song L, Liu Z, Reddy ALM et al. Direct laser writing of micro-supercapacitors on hydrated graphite oxide films. *Nat Nanotech* **6**, 496–500 (2011).
21. Kavinkumar T, Kavitha P, Naresh N, Manivannan S, Muneeswaran M et al. High performance flexible solid-state symmetric supercapacitors based on laser induced porous reduced graphene oxide-graphene oxide hybrid nanostructure devices. *Appl Surf Sci* **480**, 671–679 (2019).
22. Luo SD, Hoang PT, Liu T. Direct laser writing for creating porous graphitic structures and their use for flexible and highly sensitive sensor and sensor arrays. *Carbon* **96**, 522–531 (2016).
23. Carvalho AF, Fernandes AJS, Leitão C, Deuermeier J, Marques AC et al. Laser-induced graphene strain sensors produced by ultraviolet irradiation of polyimide. *Adv Funct Mater* **28**, 1805271 (2018).
24. Wan ZF, Umer M, Lobino M, Thiel D, Nguyen NT et al. Laser induced self-n-doped porous graphene as an electrochemical biosensor for femtomolar miRNA detection. *Carbon* **163**, 385–394 (2020).
25. Wan ZF, Nguyen NT, Gao YS, Li Q. Laser induced graphene for biosensors. *Sustain Mater Technol* **25**, e00205 (2020).
26. Li RZ, Yan J, Fang YM, Fan XY, Sheng LK et al. Laser-scribed lossy microstrip lines for radio frequency applications. *Appl Sci* **9**, 415 (2019).
27. Kang SM, Lim K, Park H, Park JB, Park SC et al. Roll-to-roll laser-printed graphene-graphitic carbon electrodes for high-performance supercapacitors. *ACS Appl Mater Interfaces* **10**, 1033–1038 (2018).
28. Zhang L, DeArmond D, Alvarez NT, Malik R, Oslin N et al. Flexible micro-supercapacitor based on graphene with 3D structure. *Small* **13**, 1603114 (2017).
29. Ye JL, Tan HB, Wu SL, Ni K, Pan F et al. Direct laser writing of graphene made from chemical vapor deposition for flexible, integratable micro-supercapacitors with ultrahigh power output. *Adva Mater* **30**, e1801384 (2018).
30. Zhang YN, Shi L, Hu DJ, Chen SR, Xie SY et al. Full-visible multifunctional aluminium metasurfaces by *in situ* anisotropic thermoplasmonic laser printing. *Nanoscale Horiz* **4**, 601–609 (2019).
31. Lin H, Jia BH, Gu M. Dynamic generation of debye diffraction-limited multifocal arrays for direct laser printing nanofabrication. *Opt Lett* **36**, 406–408 (2011).
32. Zhang YL, Guo L, Wei S, He YY, Xia H et al. Direct imprinting of microcircuits on graphene oxides film by femtosecond laser reduction. *Nano Today* **5**, 15–20 (2010).
33. Peng ZW, Lin J, Ye RQ, Samuel ELG, Tour JM. Flexible and stackable laser-induced graphene supercapacitors. *ACS Appl Mater Interfaces* **7**, 3414–3419 (2015).
34. Wu H, Zhang WL, Kandambeth S, Shekhah O, Eddaoudi M et al. Conductive metal–organic frameworks selectively grown on laser‐scribed graphene for electrochemical microsupercapacitors. *Adv Energy Mater* **9**, 1900482 (2019).
35. Rahimi R, Ochoa M, Yu WY, Ziaie B. Highly stretchable and sensitive unidirectional strain sensor via laser carbonization. *ACS Appl Mater Interfaces* **7**, 4463–4470 (2015).
36. Huang L, Liu Y, Ji LC, Xie YQ, Wang T et al. Pulsed laser assisted reduction of graphene oxide. *Carbon* **49**, 2431–2436 (2011).
37. Cheng HH, Ye MH, Zhao F, Hu CG, Zhao Y et al. A general and extremely simple remote approach toward graphene bulks with in situ multifunctionalization. *Adv Mater* **28**, 3305–3312 (2016).
38. Singh RK, Kumar R, Singh DP. Graphene oxide: strategies for synthesis, reduction and frontier applications. *RSC Adv* **6**, 64993–65011 (2016).
39. Deng NQ, Tian H, Ju ZY, Zhao HM, Li C et al. Tunable graphene oxide reduction and graphene patterning at room temperature on arbitrary substrates. *Carbon* **109**, 173–181 (2016).
40. Smirnov VA, Arbuzov AA, Shul'ga YM, Baskakov SA, Martynenko VM et al. Photoreduction of graphite oxide. *High Energy Chem* **45**, 57–61 (2011).
41. Wang GC, Yang ZY, Li XW, Li CZ. Synthesis of poly(aniline-co-o-anisidine)-intercalated graphite oxide composite by delamination/reassembling method. *Carbon* **43**, 2564–2570 (2005).
42. Wan ZF, Wang SJ, Haylock B, Kaur J, Tanner P et al. Tuning the sub-processes in laser reduction of graphene oxide by adjusting the power and scanning speed of laser. *Carbon* **141**, 83–91 (2019).
43. Wang DW, Min YG, Yu YH, Peng B. Laser induced self-propagating reduction and exfoliation of graphite oxide as an electrode material for supercapacitors. *Electrochim Acta* **141**, 271–278 (2014).
44. Hu Y, Cheng HH, Zhao F, Chen N, Jiang L et al. All-in-one graphene fiber supercapacitor. *Nanoscale* **6**, 6448–6451 (2014).
45. Shi HH, Jang S, Naguib HE. Freestanding laser-assisted reduced graphene oxide microribbon textile electrode fabricated on a liquid surface for supercapacitors and breath sensors. *ACS Appl Mater Interfaces* **11**, 27183–27191 (2019).
46. Ibrahim KH, Irannejad M, Hajialamdari M, Ramadhan A, Musselman KP et al. A novel femtosecond laser-assisted method for the synthesis of reduced graphene oxide gels and thin films with tunable properties. *Adv Mater Interfaces* **3**, 1500864 (2016).
47. Lin J, Peng ZW, Liu YY, Ruiz-Zepeda F, Ye RQ et al. Laser-induced porous graphene films from commercial polymers. *Nat Commun* **5**, 5714 (2014).
48. Ye RQ, Chyan Y, Zhang JB, Li YL, Han X et al. Laser-induced graphene formation on wood. *Adv Mater* **29**, 1702211 (2017).
49. Chyan Y, Ye RQ, Li YL, Singh SP, Arnusch CJ et al. Laser-induced graphene by multiple lasing: toward electronics on cloth, paper, and food. *ACS Nano* **12**, 2176–2183 (2018).

50. Zhang ZC, Song MM, Hao JX, Wu KB, Li CY et al. Visible light laser-induced graphene from phenolic resin: a new approach for directly writing graphene-based electrochemical devices on various substrates. *Carbon* **127**, 287–296 (2018).
51. Cao LJ, Zhu SR, Pan BB, Dai XY, Zhao WW et al. Stable and durable laser-induced graphene patterns embedded in polymer substrates. *Carbon* **163**, 85–94 (2020).
52. Lamberti A, Serrapede M, Ferraro G, Fontana M, Perrucci F et al. All-SPEEK flexible supercapacitor exploiting laser-induced graphenization. *2D Mater* **4**, 035012 (2017).
53. Zhang WL, Lei YJ, Ming FW, Jiang Q, Costa PMFJ et al. Lignin laser lithography: a direct-write method for fabricating 3D graphene electrodes for microsupercapacitors. *Adv Energy Mater* **8**, 1801840 (2018).
54. Strauss V, Marsh K, Kowal MD, El-Kady M, Kaner RB. A simple route to porous graphene from carbon nanodots for supercapacitor applications. *Adv Mater* **30** (2018).
55. Zhang JH, Zhou T, Wen L, Zhang AM. Fabricating metallic circuit patterns on polymer substrates through laser and selective metallization. *ACS Appl Mater Interfaces* **8**, 33999–34007 (2016).
56. Cai JG, Lv C, Watanabe A. Laser direct writing and selective metallization of metallic circuits for integrated wireless devices. *ACS Appl Mater Interfaces* **10**, 915–924 (2018).
57. Liu HL, Tang Y, Xie YX, Lu LS, Wan ZP et al. Effect of pulsed ND:YAG laser processing parameters on surface properties of polyimide films. *Surf Coat Technol* **361**, 102–111 (2019).
58. Yang DF, Bock C. Laser reduced graphene for supercapacitor applications. *J Power Sources* **337**, 73–81 (2017).
59. Lamberti A, Perrucci F, Caprioli M, Serrapede M, Fontana M et al. New insights on laser-induced graphene electrodes for flexible supercapacitors: tunable morphology and physical properties. *Nanotechnology* **28**, 174002 (2017).
60. Tiliakos A, Ceaus C, Iordache SM, Vasile E, Stamatin I. Morphic transitions of nanocarbons via laser pyrolysis of polyimide films. *J Anal Appl Pyrolysis* **121**, 275–286 (2016).
61. Tran TX, Choi H, Che CH, Sul JH, Kim IG et al. Laser-induced reduction of graphene oxide by intensity-modulated line beam for supercapacitor applications. *ACS Appl Mater Interfaces* **10**, 39777–39784 (2018).
62. Fu XY, Zhang YL, Jiang HB, Han DD, Liu YQ et al. Hierarchically structuring and synchronous photoreduction of graphene oxide films by laser holography for supercapacitors. *Opt Lett* **44**, 1714–1717 (2019).
63. Guan YC, Fang YW, Lim GC, Zheng HY, Hong MH. Fabrication of laser-reduced graphene oxide in liquid nitrogen environment. *Sci Rep* **6**, 28913 (2016).
64. Li YL, Luong DX, Zhang JB, Tarkunde YR, Kittrell C et al. Laser-induced graphene in controlled atmospheres: from superhydrophilic to superhydrophobic surfaces. *Adv Mater* **29**, 1700496 (2017).
65. Huang Y, Liang JJ, Chen YS. An overview of the applications of graphene-based materials in supercapacitors. *Small* **8**, 1805–1834 (2012).
66. Snook GA, Kao P, Best AS. Conducting-polymer-based supercapacitor devices and electrodes. *J Power Sources* **196**, 1–12 (2011).
67. Zhang LL, Zhao XS. Carbon-based materials as supercapacitor electrodes. *Chem Soc Rev* **38**, 2520–2531 (2009).
68. El-Kady MF, Strong V, Dubin S, Kaner RB. Laser scribing of high-performance and flexible graphene-based electrochemical capacitors. *Science* **335**, 1326–1330 (2012).
69. El-Kady MF, Kaner RB. Scalable fabrication of high-power graphene micro-supercapacitors for flexible and on-chip energy storage. *Nat Commun* **4**, 1475 (2013).
70. Li RZ, Peng R, Kihm KD, Bai S, Bridges D et al. High-rate in-plane micro-supercapacitors scribed onto photo paper using *in situ* femtolaser-reduced graphene oxide/Au nanoparticle microelectrodes. *Energy Environ Sci* **9**, 1458–1467 (2016).
71. Peng ZW, Ye RQ, Mann JA, Zakhidov D, Li YL et al. Flexible boron-doped laser-induced graphene microsupercapacitors. *ACS Nano* **9**, 5868–5875 (2015).
72. Wen FS, Hao CX, Xiang JY, Wang LM, Hou H et al. Enhanced laser scribed flexible graphene-based micro-supercapacitor performance with reduction of carbon nanotubes diameter. *Carbon* **75**, 236–243 (2014).
73. Li XQ, Cai WH, Teh KS, Qi MJ, Zang XN et al. High-voltage flexible microsupercapacitors based on laser-induced graphene. *ACS Appl Mater Interfaces* **10**, 26357–26364 (2018).
74. Thekkekara LV, Gu M. Bioinspired fractal electrodes for solar energy storages. *Sci Rep* **7**, 45585 (2017).
75. Li L, Zhang JB, Peng ZW, Li YL, Gao CT et al. High-performance pseudocapacitive microsupercapacitors from laser-induced graphene. *Adv Mater* **28**, 838–845 (2016).
76. Liu HL, Moon KS, Li JX, Xie YX, Liu J et al. Laser-oxidized Fe_3O_4 nanoparticles anchored on 3D macroporous graphene flexible electrodes for ultrahigh-energy in-plane hybrid microsupercapacitors. *Nano Energy* **77**, 105058 (2020).
77. Liu CL, Liang HW, Wu D, Lu XY, Wang Q. Direct semiconductor laser writing of few-layer graphene polyhedra networks for flexible solid-state supercapacitor. *Adv Electron Mater* **4**, 1800092 (2018).
78. Xie BH, Wang Y, Lai WH, Lin W, Lin ZY et al. Laser-processed graphene based micro-supercapacitors for ultrathin, rollable, compact and designable energy storage components. *Nano Energy* **26**, 276–285 (2016).
79. Shen DZ, Zou GS, Liu L, Zhao WZ, Wu AP et al. Scalable high-performance ultraminiature graphene micro-supercapacitors by a hybrid technique combining direct writing and controllable microdroplet transfer. *ACS Appl Mater Interfaces* **10**, 5404–5412 (2018).
80. Thekkekara LV, Chen X, Gu M. Two-photon-induced stretchable graphene supercapacitors. *Sci Rep* **8**, 11722 (2018).
81. Zhang WL, Lei YJ, Jiang Q, Ming FW, Costa PMFJ et al. 3D laser scribed graphene derived from carbon nanospheres: an ultrahigh‐power electrode for supercapacitors. *Small Methods* **3**, 1900005 (2019).
82. Kwon S, Yoon Y, Ahn J, Lim H, Kim G et al. Facile laser fabrication of high quality graphene-based microsupercapacitors with large capacitance. *Carbon* **137**, 136–145 (2018).
83. Kamboj N, Purkait T, Das M, Sarkar S, Hazra KS et al. Ultralong cycle life and outstanding capacitive performance of a 10.8 V metal free micro-supercapacitor with highly conducting and robust laser-irradiated graphene for an integrated storage device. *Energy Environ Sci* **12**, 2507–2517 (2019).
84. Liu ZW, Peng F, Wang HJ, Yu H, Zheng WX et al. Phosphorus-doped graphite layers with high electrocatalytic activity for the O_2 reduction in an alkaline medium. *Angew Chem Int Ed* **50**, 3257–3261 (2011).

85. Yang Z, Yao Z, Li GF, Fang GY, Nie HG et al. Sulfur-doped graphene as an efficient metal-free cathode catalyst for oxygen reduction. *ACS Nano* **6**, 205–211 (2012).
86. Wu ZS, Winter A, Chen L, Sun Y, Turchanin A et al. Three-dimensional nitrogen and boron Co-doped graphene for high-performance all-solid-state supercapacitors. *Adv Mater* **24**, 5130–5135 (2012).
87. Fu XY, Chen DL, Liu Y, Jiang HB, Xia H et al. Laser reduction of nitrogen-rich carbon nanoparticles@graphene oxides composites for high rate performance supercapacitors. *ACS Appl Nano Mater* **1**, 777–784 (2018).
88. Wang FC, Dong X, Wang KD, Duan WQ, Gao M et al. Laser-induced nitrogen-doped hierarchically porous graphene for advanced electrochemical energy storage. *Carbon* **150**, 396–407 (2019).
89. Liu HL, Xie YX, Liu JB, Moon KS, Lu LS et al. Laser-induced and KOH-activated 3D graphene: a flexible activated electrode fabricated via direct laser writing for in-plane micro-supercapacitors. *Chem Eng J* **393**, 124672 (2020).
90. Fang Y, Luo B, Jia YY, Li XL, Wang B et al. Renewing functionalized graphene as electrodes for high‐performance supercapacitors. *Adv Mater* **24**, 6348–6355 (2012).
91. Amiri MH, Namdar N, Mashayekhi A, Ghasemi F, Sanaee Z et al. Flexible micro supercapacitors based on laser-scribed graphene/ZnO nanocomposite. *J Nanopart Res* **18**, 237 (2016).
92. Lee SM, Park YJ, Kim JH. Laser reduction of Zn-infiltrated multilayered graphene oxide as electrode materials for supercapacitors. *ACS Appl Nano Mater* **2**, 3711–3717 (2019).
93. Fu XY, Chen ZD, Zhang YL, Han DD, Ma JN et al. Direct laser writing of flexible planar supercapacitors based on GO and black phosphorus quantum dot nanocomposites. *Nanoscale* **11**, 9133–9140 (2019).
94. Li GJ, Mo XY, Law WC, Chan KC. 3D printed graphene/nickel electrodes for high areal capacitance electrochemical storage. *J Mater Chem A* **7**, 4055–4062 (2019).
95. Wang WT, Lu LS, Xie YX, Wu WB, Liang RX et al. Controlling the laser induction and cutting process on polyimide films for kirigami-inspired supercapacitor applications. *Sci China Technol Sci* **64**, 651–661 (2020).
96. Liang Y, Wang Z, Huang J, Cheng HH, Zhao F et al. Series of in-fiber graphene supercapacitors for flexible wearable devices. *J Mater Chem A* **3**, 2547–2551 (2015).
97. Xu RX, Zverev A, Hung A, Shen CW, Irie L et al. Kirigami-inspired, highly stretchable micro-supercapacitor patches fabricated by laser conversion and cutting. *Microsyst Nanoeng* **4**, 36 (2018).
98. Liu Q, Shi QW, Wang HZ, Zhang QH, Li YG. Laser irradiated self-supporting and flexible 3-dimentional graphene-based film electrode with promising electrochemical properties. *RSC Adv* **5**, 47074–47079 (2015).
99. Borenstein A, Strauss V, Kowal MD, Yoonessi M, Muni M et al. Laser-reduced graphene-oxide/ferrocene: a 3-D redox-active composite for supercapacitor electrodes. *J Mater Chem A* **6**, 20463–20472 (2018).
100. Yang SH, Liu YY, Hao YF, Yang XP, Goddard III WA et al. Oxygen-vacancy abundant ultrafine Co3O4/graphene composites for high-rate supercapacitor electrodes. *Adv Sci (Weinh)* **5**, 1700659 (2018).
101. Hondred JA, Medintz IL, Claussen JC. Enhanced electrochemical biosensor and supercapacitor with 3D porous architectured graphene *via* salt impregnated inkjet maskless lithography. *Nanoscale Horiz* **4**, 735–746 (2019).
102. Yang SH, Li Y, Sun J, Cao BQ. Laser induced oxygen-deficient TiO_2/graphene hybrid for high-performance supercapacitor. *J Power Sources* **431**, 220–225 (2019).
103. Ladrón-de-Guevara A, Boscá A, Pedrós J, Climent-Pascual E, de Andrés A et al. Reduced graphene oxide/polyaniline electrochemical supercapacitors fabricated by laser. *Appl Surf Sci* **467–468**, 691–697 (2019).
104. Cho EC, Chang-Jian CW, Syu WL, Tseng HS, Lee KC et al. PEDOT-modified laser-scribed graphene films as bginder-and metallic current collector-free electrodes for large-sized supercapacitors. *Appl Surf Sci* **518**, 146193 (2020).
105. Naoi K, Ishimoto S, Miyamoto JI, Naoi W. Second generation 'nanohybrid supercapacitor': evolution of capacitive energy storage devices. *Energy Environ Sci* **5**, 9363–9373 (2012).
106. del Pino ÁP, Ramadan MA, Lebière PG, Ivan R, Logofatu C et al. Fabrication of graphene-based electrochemical capacitors through reactive inverse matrix assisted pulsed laser evaporation. *Appl Surf Sci* **484**, 245–256 (2019).
107. Wang YG, Wang ZD, Xia YY. An asymmetric supercapacitor using RuO_2/TiO_2 nanotube composite and activated carbon electrodes. *Electrochim Acta* **50**, 5641–5646 (2005).
108. Lee SH, Kim JH, Yoon JR. Laser scribed graphene cathode for next generation of high performance hybrid supercapacitors. *Sci Rep* **8**, 8179 (2018).
109. Lee SH, Kim KY, Yoon JR. Binder- and conductive additive-free laser-induced graphene/$LiNi_{1/3}Mn_{1/3}Co_{1/3}O_2$ for advanced hybrid supercapacitors. *NPG Asia Mater* **12**, 28 (2020).
110. Clerici F, Fontana M, Bianco S, Serrapede M, Perrucci F et al. *In situ* MoS_2 decoration of laser-induced graphene as flexible supercapacitor electrodes. *ACS Appl Mater Interfaces* **8**, 10459–10465 (2016).
111. Thekkekara LV, Gu M. Large-scale waterproof and stretchable textile-integrated laser- printed graphene energy storages. *Sci Rep* **9**, 11822 (2019).
112. Lamberti A, Clerici F, Fontana M, Scaltrito L. A highly stretchable supercapacitor using laser-induced graphene electrodes onto elastomeric substrate. *Adv Energy Mater* **6**, 1600050 (2016).
113. Parmeggiani M, Zaccagnini P, Stassi S, Fontana M, Bianco S et al. PDMS/polyimide composite as an elastomeric substrate for multifunctional laser-induced graphene electrodes. *ACS Appl Mater Interfaces* **11**, 33221–33230 (2019).
114. Shao CX, Xu T, Gao J, Liang Y, Zhao Y et al. Flexible and integrated supercapacitor with tunable energy storage. *Nanoscale* **9**, 12324–12329 (2017).
115. Stanford MG, Zhang C, Fowlkes JD, Hoffman A, Ivanov IN et al. High-resolution laser-induced graphene. flexible electronics beyond the visible limit. *ACS Appl Mater Interfaces* **12**, 10902–10907 (2020).
116. Gao J, Shao CX, Shao SX, Wan F, Gao C et al. Laser-assisted large-scale fabrication of all-solid-state asymmetrical micro-supercapacitor array. *Small* **14**, e1801809 (2018).
117. Kumar R, Savu R, Joanni E, Vaz AR, Canesqui MA et al. Fabrication of interdigitated micro-supercapacitor devices by direct laser writing onto ultra-thin, flexible and free-standing graphite oxide films. *RSC Adv* **6**, 84769–84776 (2016).

118. In JB, Hsia B, Yoo JH, Hyun S, Carraro C et al. Facile fabrication of flexible all solid-state micro-supercapacitor by direct laser writing of porous carbon in polyimide. *Carbon* **83**, 144–151 (2015).
119. Wang ST, Yu YC, Li RZ, Feng GY, Wu ZL et al. High-performance stacked in-plane supercapacitors and supercapacitor array fabricated by femtosecond laser 3D direct writing on polyimide sheets. *Electrochim Acta* **241**, 153–161 (2017).
120. Yuan YJ, Jiang L, Li X, Zuo P, Xu CY et al. Laser photonic-reduction stamping for graphene-based micro-supercapacitors ultrafast fabrication. *Nat Commun* **11**, 6185 (2020).
121. Thekkekara LV, Jia BH, Zhang YN, Qiu L, Li DAN et al. On-chip energy storage integrated with solar cells using a laser scribed graphene oxide film. *Appl Phys Lett* **107**, 031105 (2015).
122. Cai JG, Lv C, Watanabe A. Laser direct writing of high-performance flexible all-solid-state carbon micro-supercapacitors for an on-chip self-powered photodetection system. *Nano Energy* **30**, 790–800 (2016).
123. Kim SL, Hsu JH, Yu C. Intercalated graphene oxide for flexible and practically large thermoelectric voltage generation and simultaneous energy storage. *Nano Energy* **48**, 582–589 (2018).
124. Liu HH, Li MP, Kaner RB, Chen SY, Pei QB. Monolithically integrated self-charging power pack consisting of a silicon nanowire array/conductive polymer hybrid solar cell and a laser-scribed graphene supercapacitor. *ACS Appl Mater Interfaces* **10**, 15609–15615 (2018).
125. Liu Q, Hao ZM, Liao XB, Pan XL, Li SX et al. Langmuir-blodgett nanowire devices for in situ probing of zinc-ion batteries. *Small* **15**, e1902141 (2019).
126. Hossain MM, Gu M. Radiative cooling: principles, progress, and potentials. *Adv Sci (Weinh)* **3**, 1500360 (2016).
127. Hossain MM, Jia BH, Gu M. A metamaterial emitter for highly efficient radiative cooling. *Adv Opt Mater* **3**, 1047–1051 (2015).
128. Zhang YN, Chen X, Cai BY, Luan HT, Zhang QM et al. Photonics empowered passive radiative cooling. *Adv Photonics Res* , 2000106 (2020).
129. Li W, Shi Y, Chen KF, Zhu LX, Fan SH. A comprehensive photonic approach for solar cell cooling. *ACS Photonics* **4**, 774–782 (2017).
130. Gu M, Fang XY, Ren HR, Goi E. Optically digitalized holography: a perspective for all-optical machine learning. *Engineering* **5**, 363–365 (2019).
131. Goi E, Chen X, Zhang QM, Cumming BP, Schoenhardt S et al. Nanoprinted high-neuron-density optical linear perceptrons performing near-infrared inference on a CMOS chip. *Light: Sci Appl* **10**, 40 (2021).
132. Goi E, Zhang QM, Chen X, Luan HT, Gu M. Perspective on photonic memristive neuromorphic computing. *PhotoniX* **1**, 3 (2020).
133. Ren HR, Shao W, Li Y, Salim F, Gu M. Three-dimensional vectorial holography based on machine learning inverse design. *Sci Adv* **6**, eaaz4261 (2020).
134. Zhang QM, Yu HY, Barbiero M, Wang BK, Gu M. Artificial neural networks enabled by nanophotonics. *Light: Sci Appl* **8**, 42 (2019).

Acknowledgements

The authors acknowledge the funding support of Zhangjiang National Innovation Demonstration Zone (ZJ2019-ZD-005). Xi Chen acknowledges the support from National Natural Science Foundation of China (Grant No. 11974247). Zhengfen Wan thanks to the support of Shanghai Super Postdoctoral Incentive Program.

Competing interests

The authors declare no competing financial interests.